POLITECNICO
MILANO 1863

SCUOLA DI INGEGNERIA INDUSTRIALE
E DELL'INFORMAZIONE

Combining yaw redirection and static axial induction in a ultimate-load-constrained wind farm control

Tesi di Laurea Magistrale in
Aeronautical Engineering - Ingegneria Aeronautica

Author: **Federico Isella**

Student ID: 10574101
Advisor: Prof. Alessandro Croce
Co-advisors: Prof. Stefano Cacciola
Academic Year: 2021-22

Abstract

While designing the layout of a wind farm, engineers pay close attention to minimizing the time the generators spend in the wake of others. This is an almost inevitable occurrence, and it becomes very relevant when dealing with dense wind farms. Under these conditions, only a fraction of the potential power is produced, sparking interest in finding a solution to this problem. The solution is wind farm control and is a collection of techniques operated by the farm control system that aim at maximizing power production. Reaching this goal often requires giving up on operating all the turbines at their maximum power configuration and looking at the farm as a whole. The most popular strategy is called wake steering, and consists of steering the most forward turbine moving the wake away from the back one. In this case the steered turbine is performing at a lower power and this improves the overall energy production. The downside of this technique is that the controlled machine may experience higher loads than the design ones. Another viable technique is the axial induction factor control, this strategy works by operating the upstream turbine at a lower power than what it is capable of, this leads to a more energetic flow and better performance from the rest of the machines. While this technique does not lead to large improvements in terms of power production it is notable because the turbines operating at a lower axial induction factor also experience less structural loads. Studies [1, 2] have shown that coupling wake steering with axial induction control, it is possible to reduce the loads when yawing to the point of getting back in the allowable load envelope for the turbine. This thesis aims to evaluate if the coupling of yaw redirection and derating can improve the overall power production of the farm while not exceeding the rated loads. The optimization has been carried out in many different conditions in terms of offset, direction of the wind, turbulence intensity, and wind speed. While this control strategy has different performances in different conditions, there is always an increase in power production that goes from 1.5% at worst to 18% at best.

Keywords: Wind farm optimization, FLORIS, Wake redirection, Axial induction factor control

Abstract in lingua italiana

Durante il processo di design di un parco eolico si presta molta attenzione alla minimizzazione del tempo che i generatori spenderanno in scia l'uno degli altri. Questo è inevitabile e può essere molto rilevante all'interno di siti densamente popolati. In queste condizioni solo una frazione dell'energia producibile viene raccolta catturando così un grande interesse nella soluzione di questo problema. La soluzione è il sistema di controllo di parco eolico, ed è una collezione di tecniche messe in atto dal controllore che massimizzano la produzione energetica. Il raggiungimento di questo obiettivo richiede l'abbandono del funzionamento di ogni macchina nella configurazione di massima potenza per guardare al parco nel suo complesso. La strategia più usata è quella di deflessione della scia che consiste nella rotazione della prima turbina spostando la scia il più lontano possibile dalla turbina sottovento. In questo caso la turbina che viene ruotata produce meno ma la produzione complessiva cresce. L'aspetto negativo di questa tecnica è che si possono generare carichi superiori di quelli di progetto. Un'altra valida tecnica è il controllo del fattore di induzione assiale, questa strategia prevede il funzionamento della turbina frontale ad una potenza minore della massima, portando ad una scia più energetica più performance delle altre macchine. Anche se l'incremento di potenza di questa strategia non è notevole, riduce notevolmente i carichi strutturali. Da studi precedenti [1, 2] è emerso che l'accoppiamento delle tecniche di deviazione della scia e controllo di induzione assiale permette di ruotare la macchina con carichi pari o inferiori al funzionamento nominale. Questa tesi mira a valutare se questa combinazione possa migliorare le prestazioni del parco eolico senza sovraccaricare le macchine. L'ottimizzazione è stata effettuata per molte diverse combinazioni di velocità del vento, distanza fra le turbine, direzione del vento ed intensità di turbolenza. Benché questa strategia porti a differenti risultati in diverse condizioni, quando entra in azione si registra come minimo un incremento dell'1.5% e al massimo un incremento del 18%.

Parole chiave: Ottimizzazione di parchi eolici, FLORIS, Deviazione di scia, Controllo del fattore di induzione assiale

Contents

Abstract **i**

Abstract in lingua italiana **iii**

Contents **v**

1 Introduction **1**
1.1 Objectives and innovative content 3
1.2 Thesis outline 4

2 Wind farm control techniques **5**
2.1 Wake Redirection 6
2.2 Axial Induction Control 8

3 Models and tools **11**
3.1 Reference wind turbine and wind farm models 11
3.2 Wind farm model FLORIS 13
3.3 Implementation of the Active Wake Redirection 15
3.4 Implementation of the Axial Induction Control 16
3.5 Workflow 17

4 Wind farm control formulation **19**
4.1 Definition of ultimate load constraints 19
4.2 Definition of simulation parameters 21
4.3 Definition of the ultimate-load-constrained wind farm control 22
4.3.1 Optimization 23
4.3.2 Yaw only unconstrained optimization 23
4.3.3 Suboptimal yaw + derating 25
4.3.4 Constrained yaw + derating 27

5 Results **31**
5.1 Parameters simulated 31
5.2 Performance of the different control strategies on model problems 31
5.2.1 Generic condition 32
5.2.2 Parametric analyses 35
5.2.3 Other cases of interest 45
5.3 Trend analysis for the optimal control 48
5.3.1 Offset 49
5.3.2 Wind speed 55
5.3.3 Impingement 59
5.3.4 Turbulence Intensity 60
5.4 Histograms 60
5.4.1 Effectiveness 61
5.4.2 Power comparison 62
5.4.3 Yaw Comparison 65
5.5 Review of the results 66

6 Conclusions **67**
6.1 Future developments 68

Bibliography **71**

A Appendix A **73**

List of Figures **81**

List of Tables **85**

List of Symbols **87**

1 | Introduction

Renewable energy technologies have increasingly gathered more attention and investment as the world is moving away from fossil fuels and towards green power. With *Fit for 55* [3] and the European Green Deal [4], the continent is placing reducing fossil fuel consumption as one of its top priorities. *Fit for 55* aims to cut by 55% all emissions by 2030, fig. 1.1 details the plans for the energy production technologies necessary to reach this target. Furthermore, the European Green Deal aims at carbon neutrality for 2050, making essential an energetic transition to renewable power production plants. As of today, wind energy and offshore farms represent the most efficient mean of generating clean energy [5], making it one of the essential technologies necessary to make the transition possible.

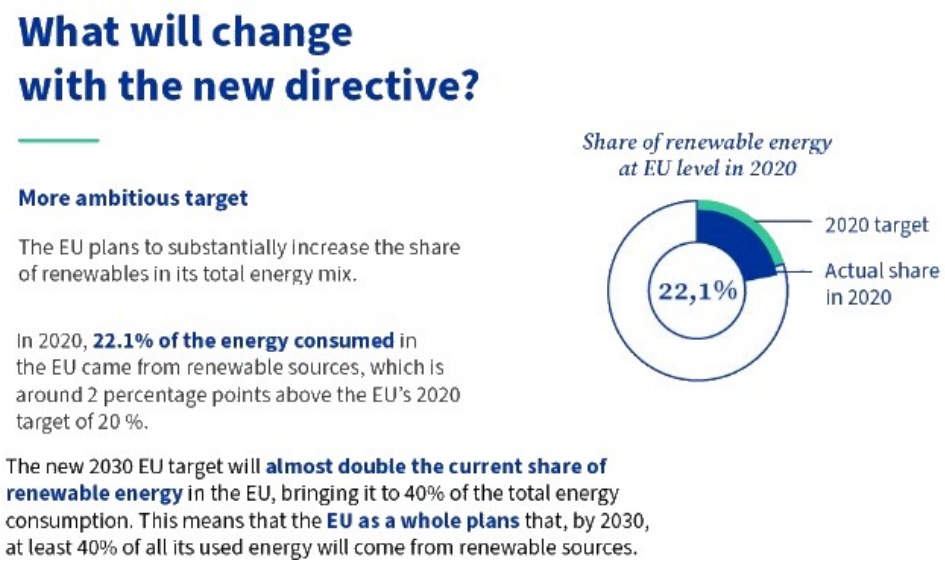

Figure 1.1: *Fit for 55* info-graphic [6] detailing the goals for renewable energy in 2030

The main advantage of wind power over the other clean energy systems is its lower cost of energy in comparison to the alternatives so much so that the European Commission stated that Europe needs between 230 and 450 GW of offshore wind by 2050 [7]. In addition to these plans, recently the price of electricity skyrocketed due to a shortage in

the supply of natural gas [8], shedding even more light on the increasingly important role that renewable power plants can fulfill. To meet these demands the wind sector focuses on building larger offshore farms, more densely packed with bigger and more powerful turbines. A prime example of this is the danish energy islands project that plans on delivering 3-4 GW of energy, with a long-term expansion potential of 10 GW in the North sea and 3 GW in the baltic sea [9]. The reason behind choosing to build large farms is that the cost of installation and infrastructure per turbine is lower when installing a large number of machines. When dealing with such a large energy production, any inefficiency builds up to a substatial amount of wasted power. One unavoidable loss comes from generators operating in the wake of others, and this phenomenon can lead to losses of up 23% of the total power generation [10]. This massive margin of improvement led engineers to formulate innovative control strategies to recover part of the energy lost. These effects impact wind turbines in terms of production losses depending on the relative position and distance of the turbines; for this reason, some farms are more affected than others. For instance, in fig. 1.2 we find an example of power production of a low-spaced farm for different wind directions.

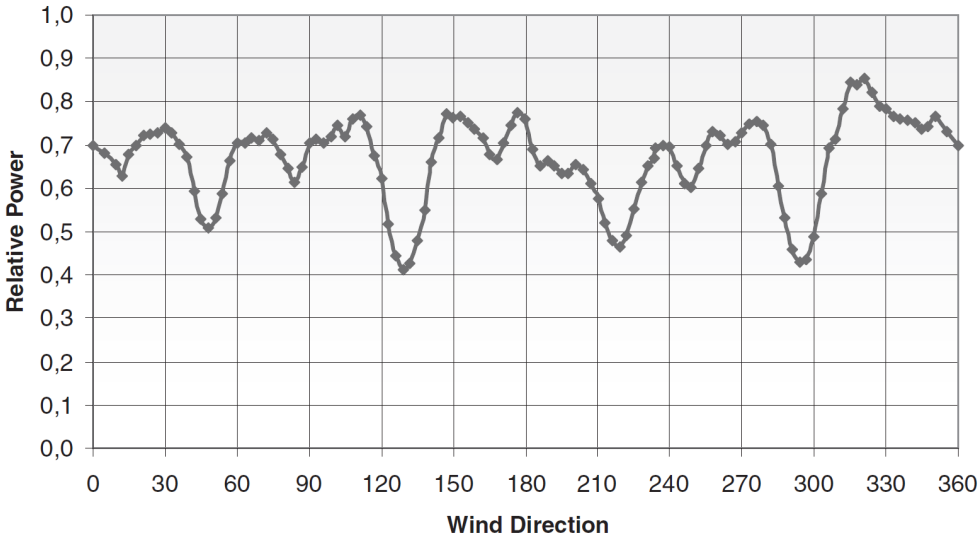

Figure 1.2: Lillground wind farm: variation in array efficiency with wind direction for wind speeds below rated. Credit to Dahlberg and Thor [11]

Strategies aimed at mitigating these losses are an active field of study; one of the most promising approaches is the Active Wake Redirection strategy. This technique is based on the fact that after a change in the direction of the rotational plane of the rotor, the wake also is deflected. This can prove helpful in solving the problem in question; the deflection of the wake can lead to the turbines in the back performing in a much cleaner wind stream

resulting in a higher power production. While simple in concept, its implementation poses some challenges in terms of structural requirements. It is possible that yawing a turbine not designed to do so can lead to excessive loads, and this must be taken into account. Another strategy used for wind farm optimization is called Axial Induction Control. It relies on the concept of derating the upstream turbines through its control system leading to less power produced but a more energetic wake. Thanks to this, the downstream turbines perform better, leading to an overall higher power production. In terms of structural loads, this strategy shows no threat of exceeding the design load envelope, as its effect is to lower the loads on the structure. It is also worth mentioning the techniques of Dynamic Induction Control; these strategies feature a specific periodic motion of the blades on their pitch axis. The effect of this movement is the production of vortexes that, through complex fluid dynamics, improve the recovery of the kinetic energy of the wake. Different cyclic movements can be used to achieve this result; most notably, a sinusoidal motion is among the most effective, while the Gaussian Periodic Collective Motion is the best. While these techniques can be accounted for during the design process, for existing wind farms the implementation of control strategies is a challenge. The possibility of the loads exceeding the design envelope is a danger that must be considered. In these cases it must be developed a technique that takes in to account both the power optimization and the structural constraints of the problem. This thesis aims to reach this goal through the combination of axial induction control and wake redirection such that the resulting technique is a viable option for implementation in all existing wind farms. A thesis [1] and an article [2] represent the starting point of this work, both from the Politecnico di Milano, that lay the foundation of the structural analysis needed to complete this thesis.

1.1. Objectives and innovative content

The objective of this thesis is the formulation and the validation, through software simulation , of a wind farm control strategy that considers the increment of the ultimate loads of the turbines controlled. The structural groundwork for this thesis has been laid out by two papers that tackle the computation of all the structural loads consequent to applying a hybrid control strategy[1, 2]. The strategy in question is a combination of yaw redirection and axial induction control, these two strategies have been applied simultaneously, and the consequent loads have been analyzed. The main result that will serve as a starting point for this work is a curve called constraint curve that allows for the definition of what combination of derating and yaw angles are compliant with the structural design of the machine. Starting from this data, this thesis will focus on the power production of a farm controlled using this strategy. A set of optimization problems

will be defined to achieve this result, and a software environment for their solution will be developed. The program used for simulating the behavior of the farm and its power output is FLORIS. This software relies on engineering models of the wake and flow field to simulate the interaction between multiple turbines in a farm. The ultimate goal is to use the results obtained by solving the optimization problems in a diverse set of conditions to conclude the effectiveness of this strategy, the conditions for which it excels, and the ones not well suited for its application. Thanks to the way the problem is posed, this thesis will also contain a comparison in performance between the hybrid strategy and the wake redirection technique.

1.2. Thesis outline

The layout of this document will be the following. Chapter 2 will be dedicated to the explanations of the prevalent wind farm control techniques, their flaws and their benefits. This chapter is essential to comprehend how the hybrid strategy discussed throughout the thesis is constructed and the reason behind its definition. Chapter 3 is going to be a presentation of the models and the tools used to set up and run all the simulations that make up the results of this paper. This chapter is going to contain both an introduction to the software used and an introduction to the software devolved and the resulting workflow. Chapter 4 is going to be dedicated to definition of the control strategy, the definition of the data obtained form previous work and, last but not least, the definition of all the optimization problems. This step is crucial as it contains the definition of the core aspect of the whole paper: in addition to solving all the optimization problems with the hybrid strategy, it will also be solved with a suboptimal approach and a unconstrained one that will serve as a comparison tool to evaluate the performances. Chapter 5 will contain the post-processed results of the 945 optimization problems. It will feature, at first, a presentation of the tools used to study the results applied to a baseline case. Moving on the same tools will be used to study the impact of the variation of the simulation parameter on the power curves. There will then be a broader look at the results to highlight trends and analyze a wider array of cases. This will be followed by the use of histogram to draw broad spectrum conclusions form the data gathered. The last section of this chapter will be dedicated to the summary of the main results. The last chapter 6 is going to contain a conclusion to this paper highlighting the main findings and laying out a path for future development on this topic. Appendix A will complement the rest of the thesis by giving a brief overview of the code used and explaining the structure of the scripts developed for this thesis.

2 | Wind farm control techniques

Farm controller systems are a part of all modern wind farms. Originally systems dedicated to over-viewing the power production facility, they had the task of detecting malfunctions, providing the turbines with anemometric data, and monitoring the overall power output to ensure it complies with the electrical network. As the complexity of the farm increased and their behavior got better understood, these systems gathered the responsibility of maximizing the farm power output. There are many different strategies to achieve this result, and they all rely on manipulating the wake of the turbines at the front to achieve better performances from the turbines in the back. Among all the methods researched today, this thesis will focus on combining wake redirection and axial induction control. This hybrid control strategy has been shown in previous studies [1, 2] to have the potential to be applied to all existing wind farms; what is left to examine, and what this thesis aims at doing, is the potential it has in terms of power production.

2.1. Wake Redirection

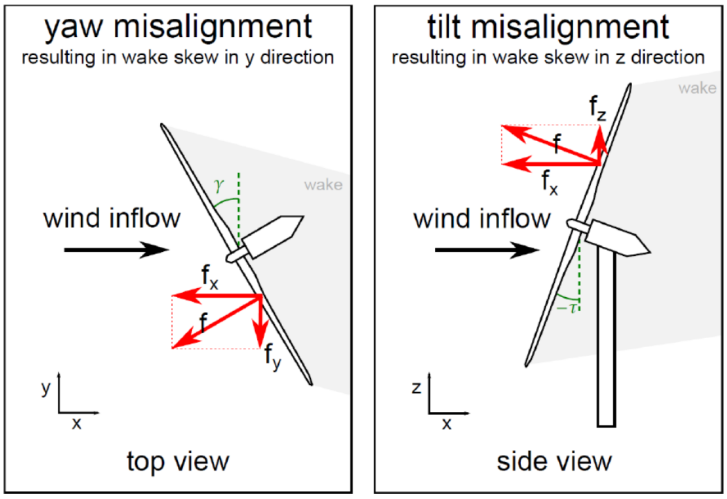

Figure 2.1: Demonstration of the yaw and tilt misalignment for wake steering. Credit to Gebraad et al. [12]

Since any misalignment of the turbine operational plane leads to lateral aerodynamic forces acting on the machine, the conservation of momentum law dictates that the same forces are applied to the wake making it not aligned with the wind direction. Moreover, changing a machine's yaw or tilt angle modifies the rotor axial induction, reducing, even more, the energy extracted from the flow, resulting in a more energetic wake. This proves advantageous because the downstream turbine can perform much better in these conditions. Fleming et al. [13] have shown an example of the potential of this strategy in fig. 2.2 where is depicted the power production of a farm constituted by two turbines operating in different conditions. When an angle of yaw or tilt is applied on the first turbine, its power output decreases, but, in most cases, the total power output is higher for the farm. Figure 2.2 also highlights an important concept: the asymmetry of the problem. Since the turbine has a direction of rotation, the wake has a swirl and naturally deflects slightly to one side. As a consequence, steering in one direction improves power production by moving the wake further away from the second turbine, but moving the turbine on the other side leads to a power decrement as the second machine is hit even more by the wake. This is one of the many effects that influence the shape of the power curve over the yaw and is a preview of the many factors that have to be considered when evaluating the behavior of the power curves of a farm.

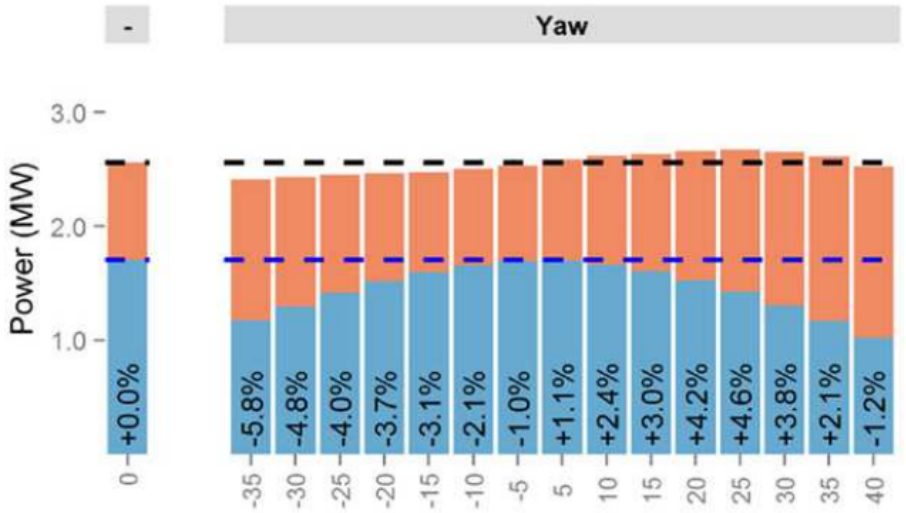

(a) Combined power output for yaw misalignment compared with the baseline case. Turbine 1 is blue, turbine 2 is orange.

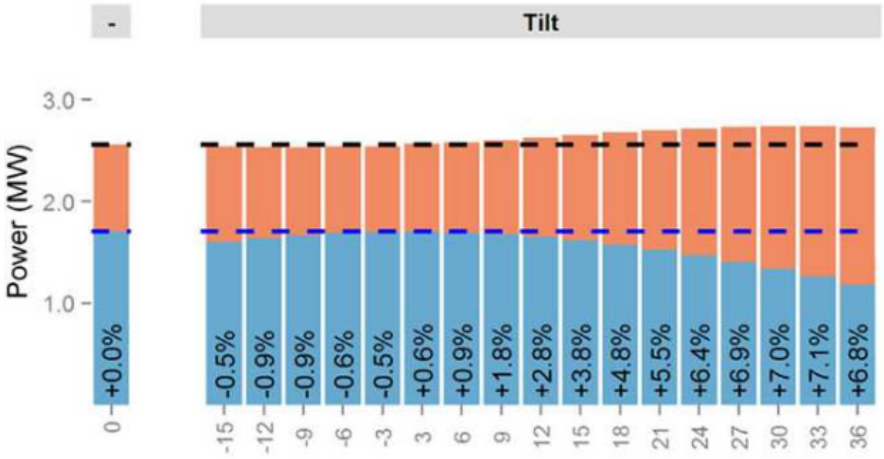

(b) Combined power output for tilt misalignment compared with the baseline case. Turbine 1 is blue, turbine 2 is orange.

Figure 2.2: Summary of the results of the two-turbine simulation. Thanks to Fleming et al. [13]

In terms of loads, it has been proven [1, 2] that this control strategy can produce stresses that exceed the rated loads for some wind turbines in specific conditions. This is expected as most wind turbines have not been designed with this control technique in mind and are optimized to function at 0° of yaw. In fact, the additional lateral loads added to the turbine's blades were not accounted for during the design process and the turbines are often designed with very small excess structural strength. It has been shown that especially in terms of chord combined momentum and maximum blade deflection, yawing the turbine leads to excessive loads. In table 2.1 are reported data for both of these load profiles in relation to the yaw angle. It is notable how there is an increase in all cases,

meaning that any misalignment from the wind direction puts the turbine outside its rated operating conditions. Another notable detail from the table in question is the asymmetry of the results; this is another consequence of the rotation of the rotor and highlights the directional nature of the problem.

Yaw Angle [°]	-25	-15	0	15	25
Maximum Tip Deflection [m]	13.56	12.90	12.63	13.54	14.83
Percentage increase in Maximum Tip Deflection [%]	7.36	2.13	0	7.20	17.41
Maximum Chord Combined Moment [MNm]	40.4	37.7	37.0	38.0	38.3
Percentage increase in Chord Combined Moment [%]	9.18	1.89	0	2.70	3.51

Table 2.1: List of the critical loads for a yawed turbine. Data credits to Dadda G. [1]

2.2. Axial Induction Control

This approach involves a change in the axial induction of an upstream generator to lower its thrust and force coefficients leading to a more energetic wake. The turbine downstream will inevitably produce more power, but this will have to counterbalance the diminished generation of the upstream machine. Since the axial induction factor a can be expressed as:

$$a = \frac{1}{2}(1 - \sqrt{1 - C_T}) \tag{2.1}$$

and $C_T = C_T(\beta, \lambda), C_P = C_P(\beta, \lambda)$ where β is the pitch and λ is the TSR. This means that to control the axial induction factor, it is necessary to change the thrust coefficient; this will also change the power coefficient and, therefore, the power production. The consequences of this chain of effects are that the effectiveness of this control strategy depends on the ratio of C_T and C_P making it not always a viable strategy for power optimization. The amount of power retrieved is also influenced by farm-specific conditions like the distance between turbines, turbulence intensity, and overlap between the wake and the second turbine. While it is a complex task to find out the effectiveness of this strategy for power optimization, applying this control technique guarantees a reduction in structural loads. Table 2.2 contains data from the same sets of simulations as the one in table 2.1 but in terms of derating instead of yaw. While the combined moment does not change, the blade deflection shows a non-negligible reduction. The idea of combining the two control strategies comes from these trends: derating while yawing the machine can reduce the load enough to get back to the rated values.

Derating [%]	0	2.5	5	10	15
Maximum Tip Deflection [m]	12.63	11.17	11.04	10.17	9.66
Percentage increase in Maximum Tip Deflection [%]	14.40	1.17	0	-7.88	-12.50
Maximum Chord Combined Moment [MNm]	37.0	37.1	37.0	37.0	37
Percentage increase in Chord Combined Moment [%]	0	0.2	0	0	0

Table 2.2: List of the critical loads for a derated turbine. Data credits to Dadda G. [1]

3 | Models and tools

3.1. Reference wind turbine and wind farm models

This thesis basis the structural analysis of the turbines on an article and a thesis [1, 2]. Both documents analyzed a farm made by two DTU 10MW wind turbines. This turbine is a popular subject among many studies because of its accessibility and traditional design, and it will also be featured in this thesis. This model has three blades and is intended for offshore use in sites with IEC wind class 1A; the rated power is 10 MW, and the NREL 5 MW reference turbine inspires its features. This machine serves the purpose of a benchmark for both aerodynamic and structural tools; its rotor has good aerodynamic performance and is lightweight, making the design a meaningful approximation of a state-of-the-art wind turbine. It is worth pointing out that this machine has never been meant to be manufactured; it is exclusively a representative design basis for research with a shared and publicly available description of its components. Table 3.1 contains the main design features of the machine. To reduce the weight of the rotor, one standard method is to increase the relative thickness of the airfoils to stiffen the blade. For this reason, the rotor features FFA-W3-xxx series airfoils; this particular profile is frequently used in modern wind turbines because of their high relative thickness while still being aerodynamically efficient. They are an excellent choice for this turbine because their properties are publicly available; even the wind tunnel test results for the FFA-W3 series performed at a Reynolds number of Re=1.6x106 with high turbulence intensity. In addition to those tests, 2D computations using XFOIL have also been conducted between 9x106 and 1.3x107 and then corrected for 3D effects. The airfoils used commonly vary from 24.1% to 36% relative thickness at the tip to a cylinder at the base. To interface the FFA-W3-360 and the cylinder, profiles of 48% and 60% relative thickness have been created by interpolation, ensuring a smooth transition between the different airfoils. However, due to numerical instabilities in several simulations, the 60% thickness airfoils have been excluded from our reference model, and the aerodynamic properties of the blade from the root to the first 48% airfoil have been obtained by direct interpolation. The blade also features a twist of decreasing intensity from root to tip. The main geometrical and aerodynamic parameters

of the airfoils are reported in table 3.2 and fig. 3.1.

Propriety	**Value**
Class and category IEC	Class 1A
Rated	Power 10 MW
Rotor orientation, configuration	Upwind, 3 blades, clockwise rotation
Control	Variable speed, collective pitch
Rotor, hub diameter	178.3 m
Hub diameter	5.6 m
Hub height	119 m
Cut-in wind speed	4 m/s
Cut-out wind speed	25 m/s
Rated wind speed	11.5 m/s
Minimum rotor speed	6 rpm
Rated rotor speed	9.6 rpm
Drive-train	Medium speed, multiple stages gearbox
Gearbox ratio	50
Rated tip speed	90 m/s
Rotor mass	228 tons
Rotor overhang	7.1 m
Nacelle uptilt, rotor precone	5°
Rotor precone	4.65°

Table 3.1: DTU 10 MW reference turbine main parameters.

#	**Airfoil**	**Thickness [%]**	**Twist [deg]**	**Spanwise position [%]**
1	Cylinder	100	14.50°	0
2	Cylinder	100	14.50°	1.74
3	FFA-W3-480	48	10.08°	20.80
4	FFA-WE-360	36	7.3°	29.24
5	FFA-WE-301	30.1	5.75°	38.76
6	FFA-W3-241	24.1	0.1°	71.78
7	FFA-W3-241	24.1	-3.43°	100

Table 3.2: List of airfoils on the DTU turbine.

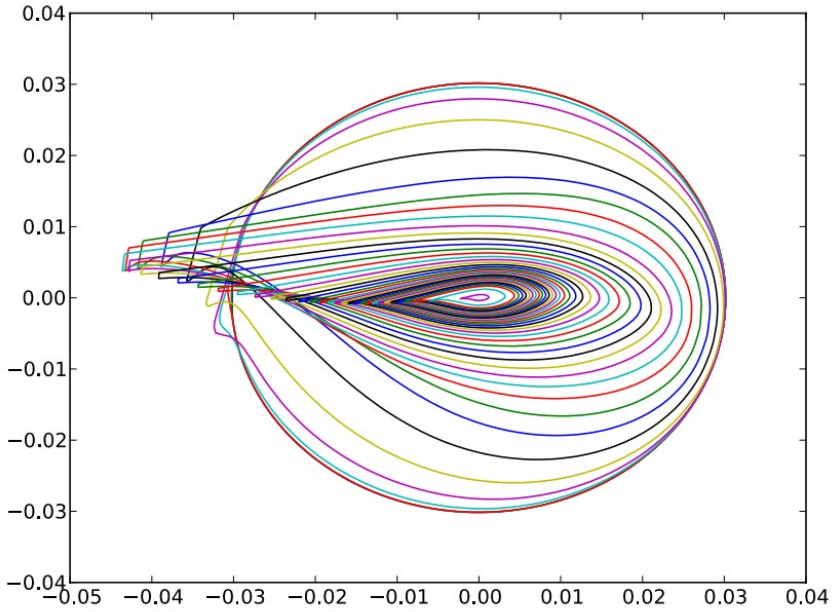

Figure 3.1: Representation of the airfoils that constitute the DTU 10 MW turbine [14]

3.2. Wind farm model FLORIS

FLOw Redirection and Induction in Steady State - FLORIS is a tool developed by NREL and Delft University of Technology with support from the U.S. Department of Energy Wind Energy Technologies Office. This software provides a computationally inexpensive modeling tool for the steady-state wake characteristics in a wind farm. The software's primary capacities are computing the operating conditions of the turbines inside of a wind farm, rendering the resulting velocity field, allowing for visualizations, and optimizing the plant's power production by computation of optimal yaw misalignment for each turbine. Both the layout of the turbines and the turbines themselves are customizable inputs of the program allowing for the modeling of any wind farm. The tool exists in MATLAB and Python; this project utilized FLORIS Version 3.0, released in February 2022 in Python. This program features many options in terms of wake modeling; fig. 3.2 depicts a collection of the four models available.

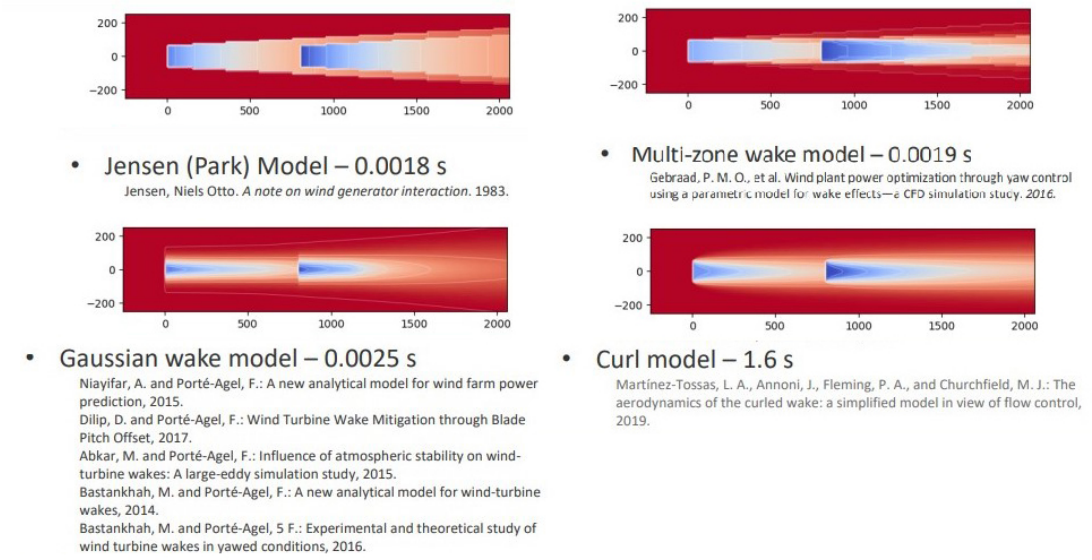

Figure 3.2: All the different wake modeling techniques implemented in FLORIS are applied to the same farm and their computational time [15]

The main models considered for this project are:

- Gaussian: based on the analytical solution to the simplified linearized Navier-Stokes equations, features four tuning parameters.
- Wake Curl: solves the linearized Navier-Stokes equations in time marching fashion, features two tuning parameters.

Both models are dependent on ambient turbulence, intensity, wind shear, and wind veer, which are site-specific parameters. Each engineering model must feature a way to model wake deflection, wake velocity deficit, wake combination, and added turbulence.

- Modeling wake deflection means describing the wake displacement caused by any misalignment between the wind direction and the turbine orientation. This works for both yaw steering and tilt steering. Depending on the model used for the simulation, the two directions can be modeled differently.
- Modeling a wake velocity deficit means computing the deceleration of the flow caused by the turbine. To calculate the velocity field downrange, wake expansion, velocity reduction, and velocity recovery must be a part of the modeled phenomena.
- Wake Combination models represent the velocity profile resulting from the mix of two or more wind streams, this includes the interaction between the wake and the free flow. This may be achieved in various ways; the main ones are velocities summation and kinetic energy summation.

- All models must consider the added turbulence; this, in practice, means modeling the increment in turbulence levels due to the interactions between the blades and the flow.

All of the aforementioned models in fig. 3.2 feature different submodels for all of these aspects and therefore generate different outputs. The more computationally expensive ones delivers more accurate results, but the key point is balancing the trade-off between accuracy and computational time according to the user's needs. Even though it is not a high-fidelity method, FLORIS has been proven to be capable of finding satisfactory results compared to experimental results [16]. The main advantage of this solution, as opposed to using a more complex aerodynamic software like CFD simulations, is the ability to run the hundreds of simulations necessary for the solution of the optimization problems in a time scale much more manageable. This allows placing more resources on simulating a larger number of conditions knowing that the validity of the results is still scientifically meaningful.

3.3. Implementation of the Active Wake Redirection

Implementing this control strategy leaves little room for interpretation; in the thesis, the angle of yaw misalignment is always defined in degrees, and the positive sign corresponds to a clockwise rotation. The software used to implement all the simulations, FLORIS, has built-in optimization routines that find the optimal yaw angle for all turbines part of the farm, therefore steering also the back one. This falls outside of the scope of this document, as introducing the additional variable of a second yaw angle would only make it harder to identify the effect of the application of the hybrid control strategy on power production. For this reason, all the optimization will be performed by an algorithm dedicated to solving the optimization problems and will not rely on any existing tool part of FLORIS. Since all the simulations are run in a steady state regime, the transition between different yaw considerations is outside the scope of this document and has not been analyzed.

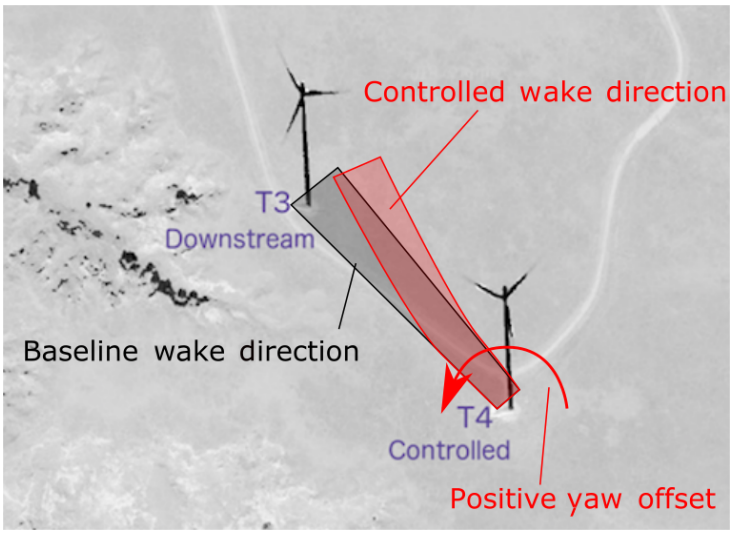

Figure 3.3: Example of yaw-based steering strategy. Credit to Fleming et al. [17].

3.4. Implementation of the Axial Induction Control

This control strategy, also called derating, can be implemented in many different ways, and its intensity is measured in percentages. Following the lead of the papers on which this document is based, the reduced Cp is computed while keeping the turbine working at a constant tip speed ratio. The new reference conditions for all wind speeds are computed starting from Cp vs TSR vs Pitch curves. The first step is the calculation of the optimal control parameters. Afterward, the power coefficient gets reduced by the desired amount allowing for the computation of new values for the pitch angle. It is also necessary to calculate the necessary values of the generator's torque to keep the power production constant while in region three. The effect of this procedure on the control variables is depicted in fig. 3.4; there, we find an example for derating 15%, where it is evident why this strategy leads to significant losses on the turbine it is implemented on. The procedure described is repeated each time a new value of derating is simulated; this is necessary because FLORIS requires Ct and Cp values as input. These coefficients get calculated starting from the output data of Cplambda simulations in regular operating conditions. The data gets then processed by a series of Matlab scripts that ultimately produce .txt files that will serve as an input for the python simulations. This means that the implementation of derating in this project is managed by Matlab while FLORIS sees a different turbine to each value of derating simulated.

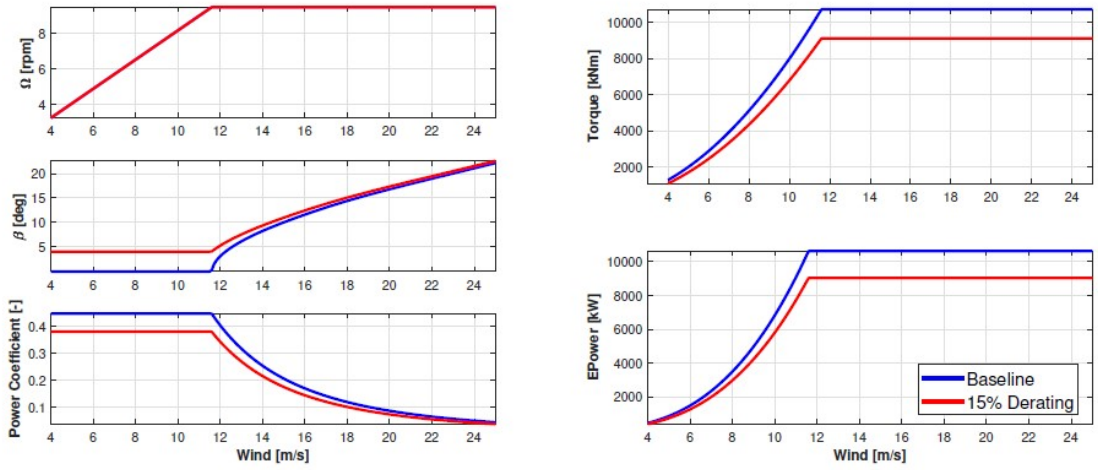

Figure 3.4: Difference in reference values from the application of 15% derating. [1]

3.5. Workflow

This section is dedicated to explaining the software framework used to run all the simulations for this project. The main challenge of this project is interfacing Matlab with FLORIS and, therefore, python. This is necessary because the post-processing of the Cplambda files is already existing in the Matlab environment, and this step is necessary for the implementation of derating; on the other hand, the most updated version of FLORIS runs through Python. It is then necessary to build a framework to make these two environments work in synergy. To achieve this, FLORIS and the Python script that runs it are being used as a 'black box': some input parameters are delivered to the script, it is run, and it outputs the desired variables back to Matlab. While it is fairly easy to make Matlab run a Python script and wait for its output, the exchange of variables between the two programs is much less intuitive. This problem is solved through the use of many, specifically formatted, .txt files; these documents get overwritten by Matlab any time a new simulation is run and contain all the parameters necessary to simulate the desired conditions. In addition to the environmental parameters, it is also necessary to deliver the necessary data to simulate the derating correctly. The input files for FLORIS are layered as follows: inside the installation folder of the package is present a turbine library, this folder is populated by files that contain all the data necessary to simulate the behavior of a given turbine, for example we can find fields about the height of the machine, its rotor dimensions, but also a list of force and power coefficients. In particular the values for Cp and Ct tabulated on the wind speed is the data that this program uses

to simulate the performance and the wake. By having a dedicated turbine file in the library folder it is possible to overwrite all of these coefficients with the ones computed during the derating calculation, therefore effectively swapping the original turbine for a new, derated, one. By acting on the input files it is possible to use the same script to simulate every condition as the parameters get changed inside its input files and not inside the script itself. A visual representation of this workflow is given in fig. 3.5 and lays out the procedure that gets run for each simulation. This means that when the optimization process is running, and multiple function evaluations are run for each condition, the only viable option is to develop a solid automation procedure like the one just described. The derating gets elaborated by a Matlab script that builds the input files for the python script, it gets run and outputs the power production of both turbines back to Matlab. This is the basic procedure used every time the power production is simulated for any reason, for this reason this routine can be seen as the heart of the computational analysis of the thesis.

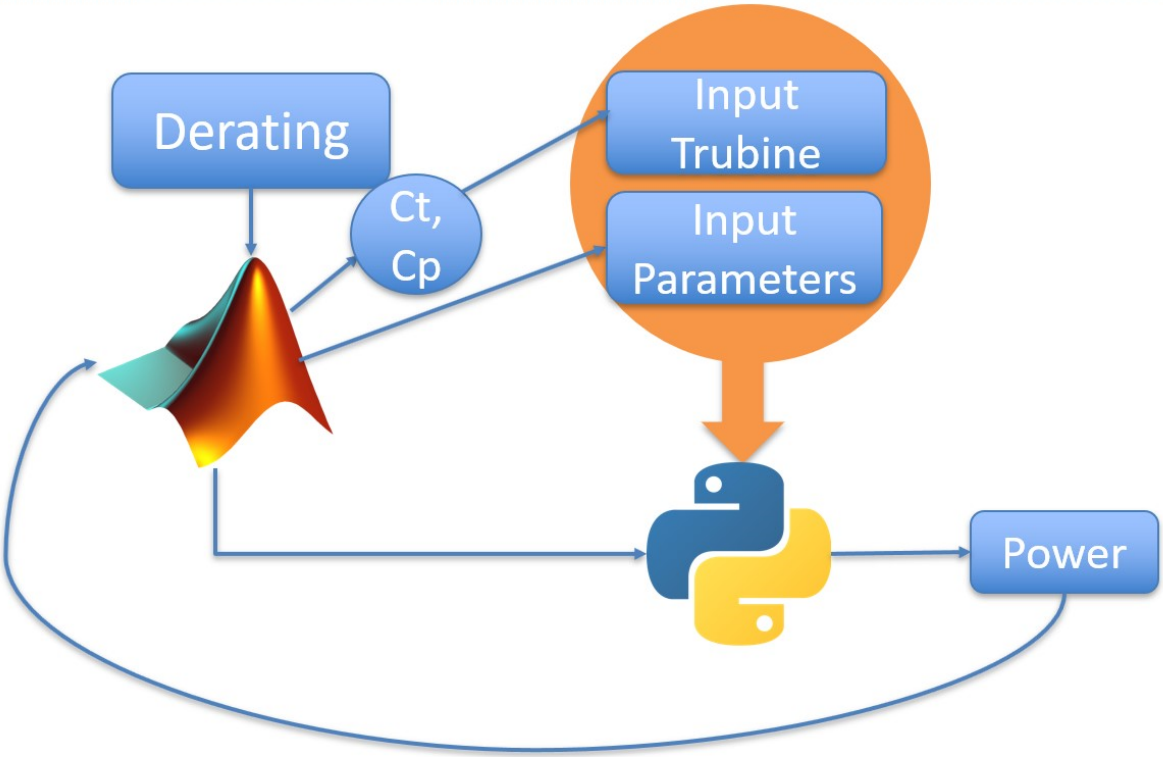

Figure 3.5: Block diagram representing the structure of the simulation script

4 | Wind farm control formulation

4.1. Definition of ultimate load constraints

A crucial part of this thesis is formulating a control strategy that complies with the structural limits of the turbines. To do this is necessary to define what conditions are allowable and what are not. This information can then be collected and represented in a curve on a plane where the axis are the control variables: this curve is the constraint curve. To better understand the meaning of the constraint curve is necessary to define it and how it is computed. During the certification process of a wind turbine is necessary to run many different aeroelastic simulations in different conditions; these simulations are called DLC, Dynamic Load Cases. Some DLCs simulate standard operating conditions, others feature gusts, and some consider failures or faults. The list of DLCs considered for computing the constraint curve is in fig. 4.1. This set of simulations is then run for each combination of yaw and derating considered in the thesis: yaw = -25° -15° 0° 15° 25°, and derating=0% 2.5% 5% 10% 15%. This means that all the DLCs listed have been performed for all twenty-five combinations of yaw and derating. Once all the data has been gathered, the maximum load registered in the baseline conditions of zero derating and zero yaw is labeled as the baseline load. The next step is looking at the maximum loads registered for each yaw value and finding the derating necessary to have the same maximum loads as the baseline case. This procedure can be carried out for all of the structural loads that the turbine experience, but the most significant that show the most increase are: the combined moment and the blade deflection. Plotting and connecting the points identified as described for these two cases leads to fig. 4.2. This graph shows the amount of derating necessary to have loads lower or equal to the baseline condition for a given yaw angle. In the spirit of applying the most conservative constraint curve available, this thesis uses a curve made of the maximum of the two: fig. 4.3. Utilizing this constraint curve is a very conservative hypothesis: the loads consequent to the same DLCs will not produce the same stress at all wind speeds. The definition of the constraint curve is a variable of the optimization strategy and different approaches to its definition may impact the results obtained. For example, a strategy to maximize power production can be computing more

constraint curves at different wind speeds leading to less demanding requirements at lower wind speeds. For the scope of this thesis, however, using the same constraint curve for all conditions does not affect the results' quality and meaning. Researching what would the impact of a different constraint curve on the power production is a good direction for future developments.

Situation	DLC	Wind type	Safety factor	Faults
Power production	1.1	NTM	1.35	No
	1.3	ETM	1.35	No
	1.4	ECD	1.35	No
Power production plus faults	2.2b	NTM	1.1	Grid loss
	2.2f	NTM	1.1	Pitch runaway
	2.3b	EOG	1.1	Grid loss

Figure 4.1: DLCs simulated for the parametric analysis. Credits to Dadda G. [1]

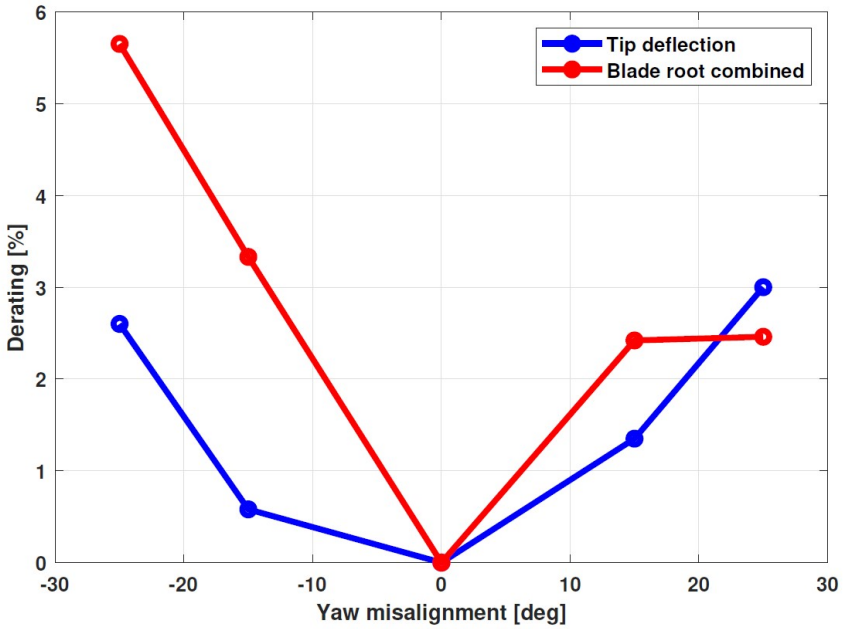

Figure 4.2: Derating needed to balance the effect of misalignment in function of the yaw angle.Blue line: maximum tip deflection. Red line: blade root combined ultimate load. [1]

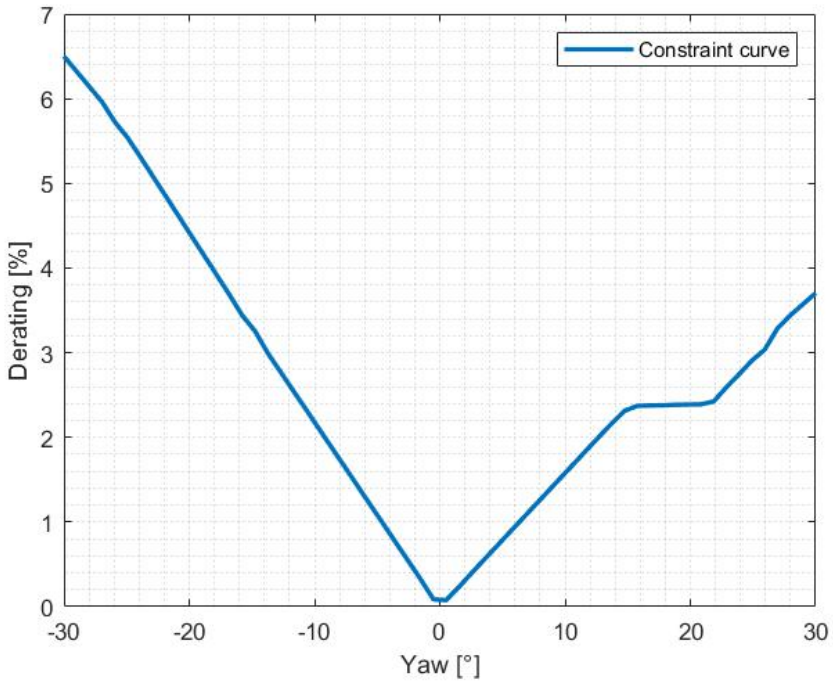

Figure 4.3: The constraint curve computed based on data presented in [1]

4.2. Definition of simulation parameters

Since this thesis aims to research the effectiveness of the combination of the two control strategies mentioned above, it is necessary to implement it in the broadest array of cases possible to reach conclusions with a wider field of relevance. To do so, the following parameters have been defined: Offset, Turbulence Intensity, Impingement, and wind speed.

- Offset: this parameter is the distance between the two turbines. It is adimensionalized over the diameter of the turbines and is therefore measured in Diameters [D].
- Turbulence Intensity: adimensional number used to describe the turbulence levels of the flow, it is often referred to as a percentage but FLORIS takes it as input in decimal form: instead of going from 0 to 100 % TI must be between 0 and 1. If the data for the site to be modeled are available only in terms of turbulence kinetic energy there are functions dedicated to perform the conversion.
- Impingement: this parameter represents winds coming at the farm from an angle.

Given the variables defined in fig. 4.4, the impingement is defined as:

$$Imp = PY/D \tag{4.1}$$

where D is the diameter of the turbine. This means that when the impingement is unitary the turbines are not overlapped on the y-axis.The main advantage of defining a parameter in such a way is the ease of relating how much a turbine is inside the wake of the other to a number that is not related to their offset.

- The wind speed is self-explanatory and a key parameter for any simulation involving wind farms and turbines. It is measured in m/s.

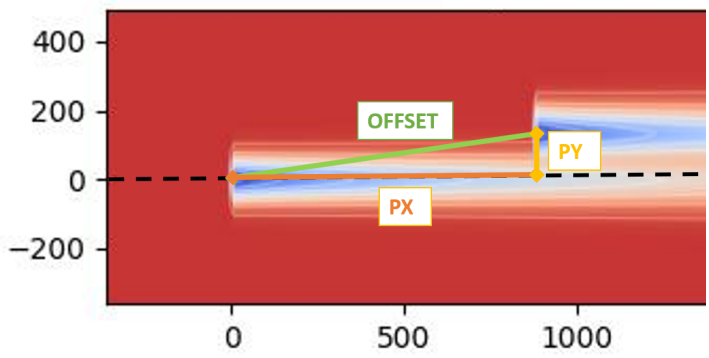

Figure 4.4: Visualization of the geometric parameters of a wind farm at impingement 0.75

To formalize the definition of these parameters as a simulation variable the vector Π of parameters is defines as such:

$$\Pi = [V, TI, Of, Im] \tag{4.2}$$

where V is the parameter Wind Speed, TI turbulence intensity, Of offset, and Im impingement. This parameter vector will be an essential part of the optimization process.

4.3. Definition of the ultimate-load-constrained wind farm control

At this point, all the foundations are in place to define the ultimate-load-constrained wind farm control. This technique aims at maximizing the power output of a wind farm while not producing greater loads than the nominal operating conditions. This goal is achieved by calculating a constraint curve through the aeroelastic simulation of many dynamic

load cases and imposing these limits to never be crossed for all operating conditions. To achieve this result, many optimization problems must be solved, and their definition will be presented in this section.

4.3.1. Optimization

Once a set of parameters has been defined, it is possible to proceed with the optimization of the power production. Since the variable to this problem are two, yaw angle and derating amount, and the solution must comply with the constraint curve, this problem is a two-variable constrained optimization problem with an adimensional power output as its objective function. The algorithm chosen for the optimization procedure is 'fmincon' from MATLAB. This gradient-based method has been set up with stopping criteria on the variables of 10^{-3}° and 0.01% derating. In order to better understand the problem analyzed, two extra optimization problems have been set up. Three optimal solutions make up the result of the optimization process for a given set of parameters: yaw only unconstrained, suboptimal yaw + derating, and constrained yaw + derating. To consider the possibility of a curve featuring multiple local optimal points, the same optimization is run three times per strategy with three different initial guesses with the goal of capturing all the local maximums.

4.3.2. Yaw only unconstrained optimization

This optimization problem only takes as a variable the yaw angle with the derating amount fixed at 0. This query aims to find the best possible power obtainable by exclusively applying the wake redirection control strategy. The objective function for this optimization problem is defined as:

$$J = -P(\widehat{\Phi}; \Pi)/\bar{P} \tag{4.3}$$

Where P is the power produced and it is a function of: adimensional yaw $\widehat{\Phi}$ defined as $\widehat{\Phi} = \Phi/F$, where F is a scalar constant of 10°, and Π is the parameter vector defined in eq. (4.2) . $\bar{P}$ is the baseline power and is the power output registered for 0° of yaw and 0% derating. Note that the objective function is negative and to the maximum of the power production corresponds the minimum of this curve, this is done because the solver looks for a minimum. The optimization problem is then defined as:

$$\widehat{\Phi}_{Opt} = arg(min(J)) \tag{4.4}$$

$$s.t. \widehat{\Phi}_{min} < \widehat{\Phi}_{Opt} < \widehat{\Phi}_{MAX} \tag{4.5}$$

$$\Phi_{opt} = \widehat{\Phi}_{Opt} F \tag{4.6}$$

$$\xi_{opt} = 0 \tag{4.7}$$

Where $\widehat{\Phi}_{Opt}$ is the optimal adimensional yaw and Φ_{Opt} is the optimal yaw, and $\xi_{opt} = 0$ is by definition of the problem the value of the derating. The domain is set as $\widehat{\Phi}_{min} = -3, \widehat{\Phi}_{MAX} = 3$ that corresponds to [-30°,30°].

It is particularly useful to look at the results of this optimization problem because it allows for the calculation of the amount of power lost to comply with the constraint curve. Since this is, in the vast majority of cases, also the overall best possible power output of the farm, it reveals the maximum effective capabilities of the control strategy, giving some context to evaluate the results of the other control strategies. In addition to the conclusion drawn by comparing the power output of the different strategies, it is also possible to look into the effect of constraining the problem in terms of optimal yaw angles.
Graphically, in a contour representation of the power curve where: the x-axis variable is the yaw angle, the y-variable is the derating, and the z-variable is the total power output of the farm, the yaw only optimization strategy deals only with the orange line in fig. 4.5. fig. 4.6 depicts the power curve on the same highlighted line; it is also notable that there may be multiple local maximums, all of which are saved to be analyzed.

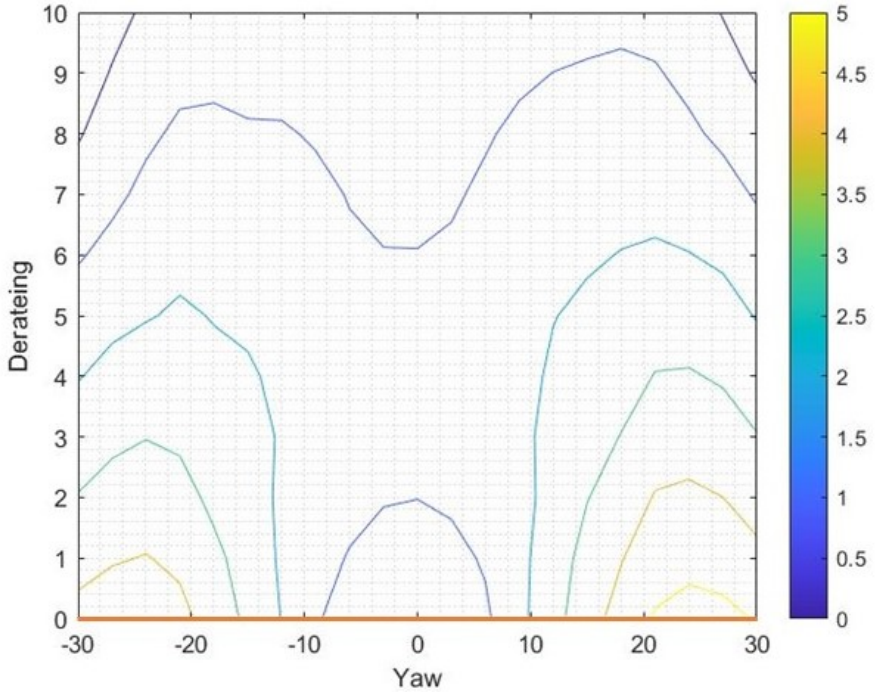

Figure 4.5: A representation of the global optimization domain, highlighting in orange the derating 0% that is the domain of the yaw-only sub-problem.

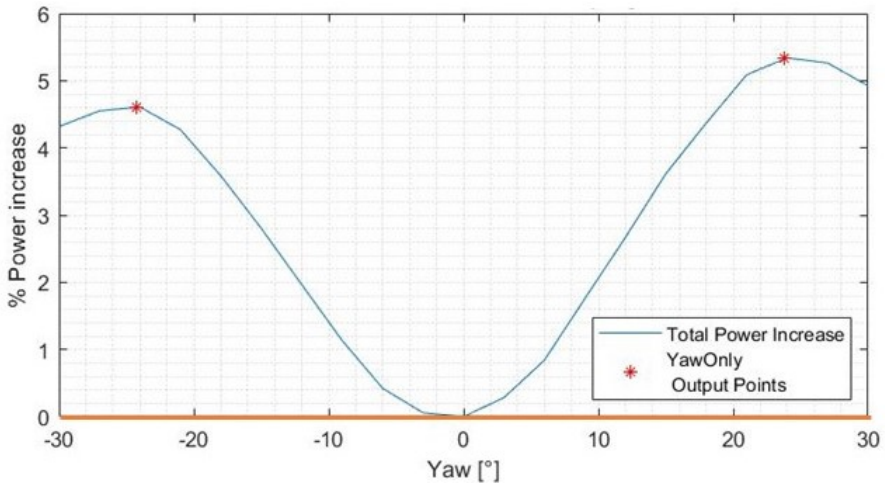

Figure 4.6: A typical power curve for derating 0% with the optimization results

4.3.3. Suboptimal yaw + derating

This optimization problem is based on starting form the yaw-only optimization and finding the derating associated to that value of yaw to build the optimal result, by definition the point calculated in such a way always lays on the constraint curve and is compliant

with the constraints. This optimization has as the only variable the yaw angle, with the derating being calculated based on the optimal yaw. The objective function for this optimization problem is defined as:

$$J = -P(\widehat{\Phi}; \Pi)/\bar{P} \tag{4.8}$$

Where P is the power produced and it is a function of: adimensional yaw $\widehat{\Phi}$ defined as $\widehat{\Phi} = \Phi/F$, where F is a scalar constant of 10°, and Π is the parameter vector defined in eq. (4.2) . $\bar{P}$ is the baseline power and is the power output registered for 0° of yaw and 0% derating. Note that the objective function is negative and to the maximum of the power production corresponds the minimum of this curve, this is done because the solver looks for a minimum. The optimization problem is then defined as:

$$\widehat{\Phi}^*_{Opt} = arg(min(J)) \tag{4.9}$$

$$s.t. \widehat{\Phi}_{min} < \widehat{\Phi}^*_{Opt} < \widehat{\Phi}_{MAX} \tag{4.10}$$

$$\Phi_{opt} = \widehat{\Phi}_{Opt} F \tag{4.11}$$

$$\xi_{opt} = Con(\widehat{\Phi}^*_{Opt}) \tag{4.12}$$

Where $\widehat{\Phi}_{Opt}$ is the optimal adimensional yaw and Φ_{Opt} is the optimal yaw, $\xi_{opt} = Con(\widehat{\Phi}^*_{Opt})$ is by definition of the problem the value of the derating. The function 'Con' is the mathematical expression of the constraint cure and is a one-variable function that takes an asimensional yaw as input and outputs the minimum allowable derating. The domain is set as $\widehat{\Phi}_{min} = -3, \widehat{\Phi}_{MAX} = 3$ that corresponds to [-30°,30°];

This optimization aims to determine if it is worth setting up the full-scale optimization problem or if this strategy can be a viable and simpler alternative. In practice, this strategy can be visualized as the projection of the yaw-only result on the constraint curve. There is no mathematical or physical proof that this leads to optimal solutions; therefore, it is necessary to research this topic to evaluate the viability of this strategy. By analyzing numerous simulation results, this thesis will present how accurate this result is and how much power is sacrificed by taking this much more straightforward and less computationally complex approach. A graphic representation of the process is provided in fig. 4.7, here it is pictured the process of projecting the optimal values of the yaw only strategy on the constraint curve. Suppose the difference between this strategy and the complete one is minimal or deemed an acceptable approximation. In that case, this strategy can be used as a tool to simplify problems that involve more variables than the one considered here, leading to faster and more efficient computational analysis.

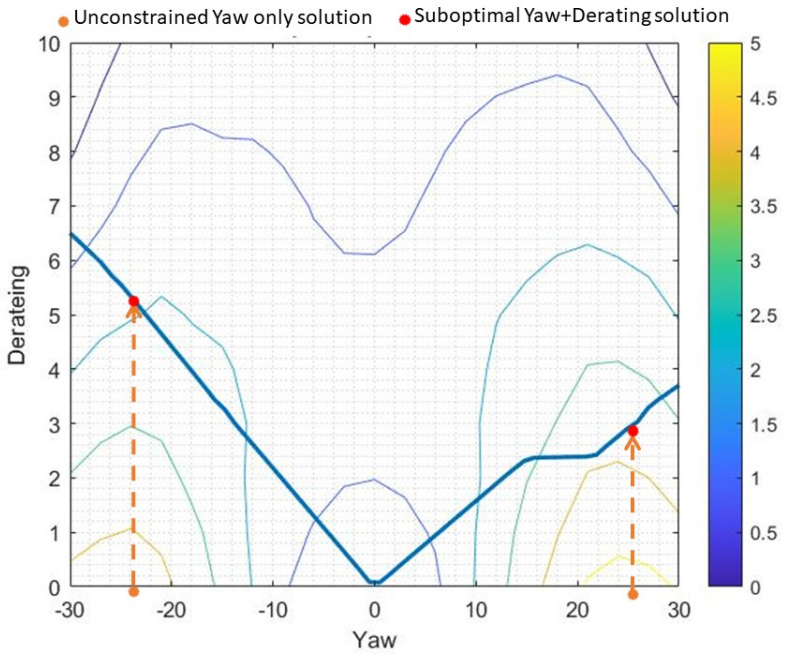

Figure 4.7: Graphical representation of the construction of the solution of the suboptimal yaw+derating optimization problem starting from the solution of the yaw-only problem

4.3.4. Constrained yaw + derating

This optimization problem is the core of the thesis as it is the mathematical formulation of the hybrid control strategy discussed in this document. This is a two-variable constrained optimization problem that has yaw angle and derating as its variables. The objective function for this optimization problem is defined as:

$$J = -P(\widehat{\Phi}, \xi; \Pi)/\bar{P} \tag{4.13}$$

Where P is the power produced and it is a function of: adimensional yaw $\widehat{\Phi}$ defined as $\widehat{\Phi} = \Phi/F$, where F is a scalar constant of 10°, ξ is the derating and ranges from 0 to 1, and Π is the parameter vector defined in eq. (4.2). $\bar{P}$ is the baseline power and is the power output registered for 0° of yaw and 0% derating. Note that the objective function is negative and to the maximum of the power production corresponds the minimum of this curve, this is done because the solver looks for a minimum. The optimization problem is then defined as:

$$(\widehat{\Phi}^*_{Opt}, \xi_{opt}) = arg(min(J)) \tag{4.14}$$

$$s.t. \widehat{\Phi}_{min} < \widehat{\Phi}^*_{Opt} < \widehat{\Phi}_{MAX} \tag{4.15}$$

$$s.t. \widehat{\xi}_{Opt} > Con(\widehat{\Phi}^*_{Opt}) \tag{4.16}$$

$$\Phi_{opt} = \widehat{\Phi}_{Opt} F \tag{4.17}$$

$$\xi_{opt} = \xi_{opt} \tag{4.18}$$

Where $\widehat{\Phi}_{Opt}$ is the optimal adimensional yaw and Φ_{Opt} is the optimal yaw, ξ_{opt} is by definition the optimal derating value. The function 'Con' is the mathematical expression of the constraint cure and is a one-variable function that takes adimensional yaw as input and outputs the minimum allowable derating. The domain is set as $\widehat{\Phi}_{min} = -3, \widehat{\Phi}_{MAX} = 3$ that corresponds to [-30°,30°];

This optimization problem is the most complex one of the three. Here both variables, as well as the constraint curve, are considered. The solution to this problem is, by definition, the best possible power output that belongs to the feasible region. This is the main result of the thesis and, compared to the other optimization outputs, allows us to reach an in-depth understanding of the effect of this hybrid control technique. By comparing these results to yaw-only ones, it is possible to figure out what is sacrificed to comply with the constraints. The comparison with the second one highlights how much improvement comes with the added computational complexity. It may be valuable to opt for the less computationally expensive if the tradeoff is considered acceptable if this technique is applied to more complex farms with way more variables. Graphically, the solution to the constrained yaw+derating problem is finding the maximum of the objective function in the field highlighted in fig. 4.8. In general, the expected result is for the unconstrained yaw-only solution to be the one that produces the highest power output; there are, however, exceptions to this that will be pointed out while discussing the results.

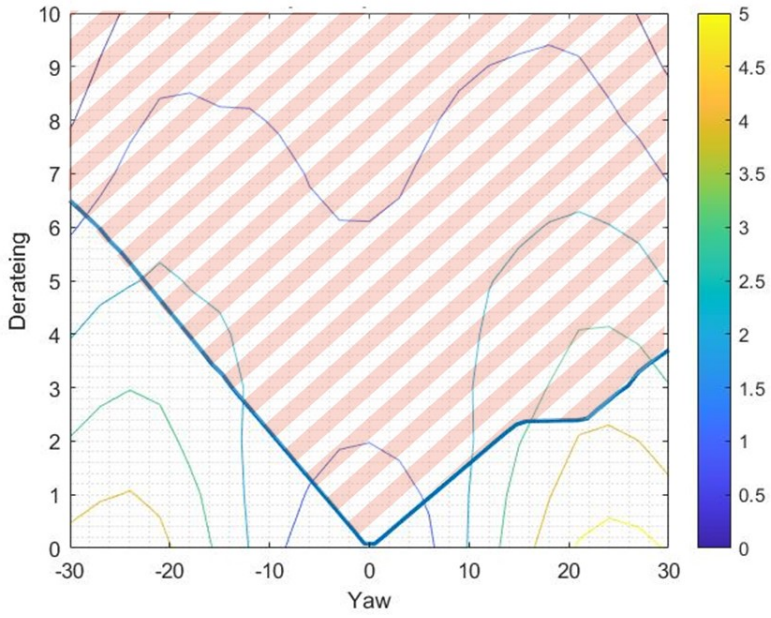

Figure 4.8: The constraint curve is overlapped on the domain of the optimization problem revealing the feasible region; this is the domain of the constrained yaw+derating optimization problem

5 | Results

5.1. Parameters simulated

As previously mentioned, this thesis involves the analysis of multiple operating conditions. The set of parameters chosen is the following:

- Offset = [3 4 5 6 7] D
- Wind Speed = [7 10 11.4 12 12.5 13 14] m/s
- Impingement = [-1 -0.75 -0.5 -0.25 0 0.25 0.5 0.75 1]
- TI = [0.02 0.06 0.1]

The total combinations of parameters amount to 945 different conditions. The main goal of this chapter is to compare the results of the three different optimization problems and to highlight the effects of the variation of each parameter on the effectiveness of this hybrid control strategy.

5.2. Performance of the different control strategies on model problems

Power curves are tridimensional graphs used for the visualization of the power output of the farm. The variables are yaw angle on the x-axis, derating on the y-axis, and PPI on the z-axis. The definition of PPI: Percentage Power Increase, is

$$PPI = \frac{OP - BP}{BP} \tag{5.1}$$

where OP is the power produced by applying the optimization strategy analyzed, and BP is the baseline power: the power produced with 0% derating and 0° of yaw. The advantage of using PPI as the power variable is that its value is 0 for 0% derating and 0° of yaw, helping to visualize more clearly the effect of the control strategy on the power produced. This 3D graph makes it possible to extrapolate two bidimensional curves of great interest

for the optimization process: the yaw-only curve for derating 0 and the constrained curve. As mentioned before, the yaw-only curve represents the PPI, considering only yaw as a variable. The constrained curve is the intersection between the PPI surface of the 3D graph and the constraint curve. Compared to the yaw-only curve, the product of this intersection shows the effect of constraining the problem on the available PPI and sheds light on the importance of the shape of the constraint curve.

5.2.1. Generic condition

To familiarize and comprehend the core aspects of the problem, the power curves of a general configuration of the farm will be analyzed. The following set of parameters will serve as a base: Wind Speed 11.4 m/s, Offset 5D, Turbulence Intensity 0.06, and Impingement 0.
These values have been chosen because they represent the median value of the sets used for the simulations. In fig. 5.2 is depicted the 3D graph for this configuration with the constraint curve overlapped on it. The first remark about this graph is how the derating, in these conditions, has a strictly decremental effect on the PPI when the tribune is steered for at least ± 10; this means that the coupling of the two strategies does not give an advantage in terms of power production. It is also of note that there are two local maximums that derive from the possibility of steering the wake on both sides of the turbine on the back; this is confirmed by fig. 5.1 which is a contour plot of the same graph. It is clear that the yaw-only strategy on the 0% derating line is the one that yields the better results. To dive deeper on that topic fig. 5.3 contains the power curve on the yaw axis, this figure highlights the two local maximums and the asymmetry of the problem: the two maximums are located within one degree of one another but lead to much different performance. This is due to the contribution of the natural wake rotation derived by the rotor's motion and always leads to more favorable results for positive steering.

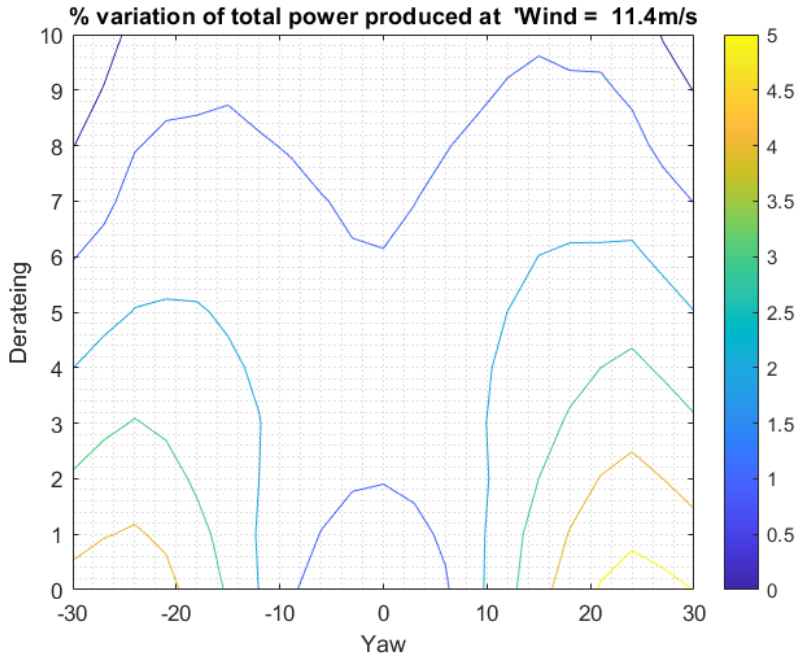

Figure 5.1: Contour plot of the PPI surface in Baseline conditions

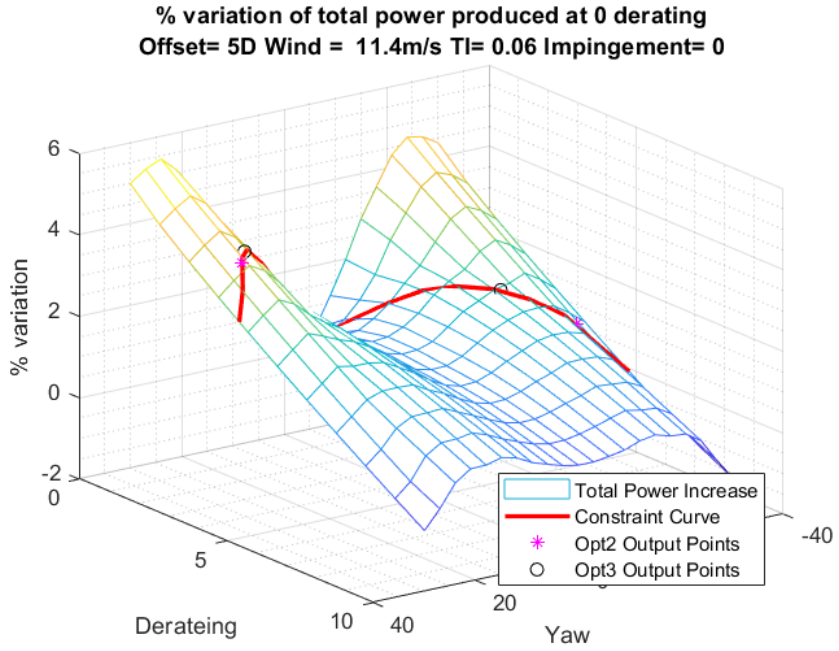

Figure 5.2: 3D surface graph of the PPI surface in Baseline conditions

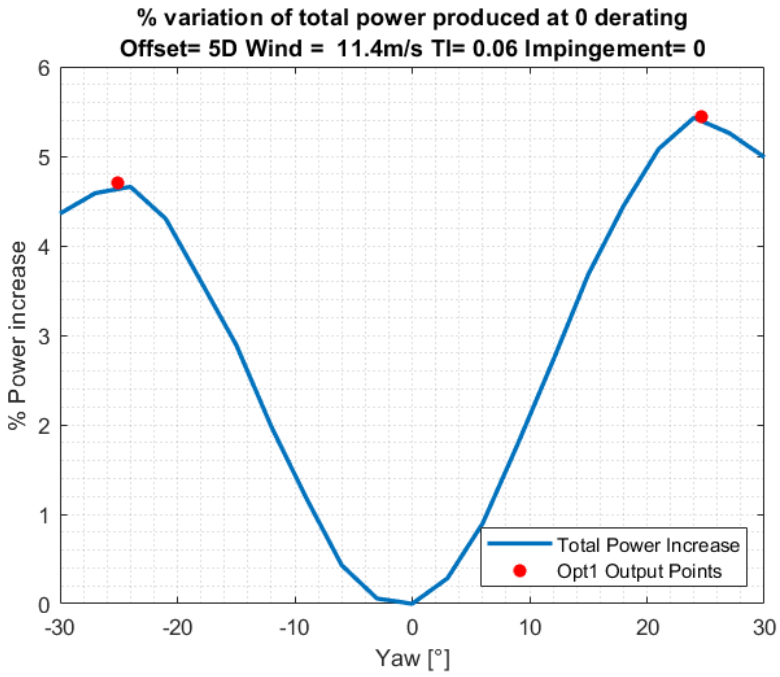

Figure 5.3: 0 Derating power curve in baseline conditions

Moving on to the constrained power curve in fig. 5.4, things differ from the 0% derating case. While in this case, there are also two local maximums, they are much less comparable in terms of PPI. The ununiform scaling of the curve is due to the asymmetry of the constraint curve and the asymmetry of the PPI surface. This means that for different-shaped constraint curves or some combinations of parameters, the absolute maximum shifts form a positive rotation to a negative or vice versa. The introduction of uneven scaling due to the constraint curve also affects the optimal yaw angle. This is to be attributed to the fact that while the optimal yaw remains such across the whole domain this is true only for the same derating amount. In this case though, the constraint curve does not operate in such a way. Lower yaw angles always correspond to a lower derating necessary; therefore, the optimal angle shifts to lower values when considering the complete problem.

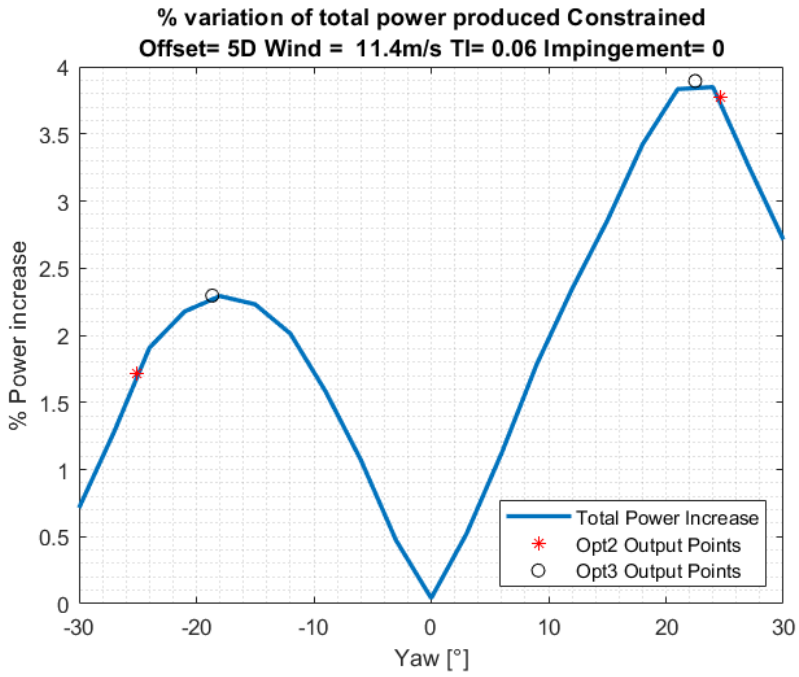

Figure 5.4: Constrained power curve in baseline conditions

While this baseline case is filled with important information, it is also essential to analyze the effect of the variation of the parameters on these curves. For each parameter, there will be a representation of the a parametric graph showing how the power curve changes when a parameter changes, with all the others fixed as the baseline ones. While this analysis does not cover the whole spectrum of simulations considered in this paper, it will allow for a better understanding of the rest of the contents of the thesis.

5.2.2. Parametric analyses

To inspect the effect of the change of the parameters on the power curves, it is useful to use parametric plots. This figure contains the power curves for all values of one parameter overlaid on top of the same plane. With this tool, it is possible to visualize how the power generation is linked to a specific propriety giving an insight into what phenomena lead to the results of the optimization process.

The effect of the variation of the impingement on the power curve is depicted in fig. 5.5. Since this parameter describes the relative position of the two tribunes, it is expected to be very disruptive on the shape power curve because it is heavily linked to the yaw as a variable. The first thing to be noted is that only the 0 impingement case leads to a curve with two maximums; all other cases show only one maximum. The reason for this is that if part of the turbine is already out of the wake, steering in one direction

will free up even more the rotor, while going in the other direction will cover up the turbine leading to worst performances. Another interesting remark on this point is how the increase in performance is much greater for lower amounts of impingement; this is due to the fact that most of the turbine is still affected by the wake leaving a large margin for improvement. When the values of impingement are closer to the unity, it means that the rotor is operating mostly in fresh air leading to a small room for improvements. This graph also confirms the asymmetry of the problem, it is notable how all the curves with positive impingement (with maximums on the positive side) show a higher PPI in four out of four cases with higher values of impingement having less difference between each other. This is consistent with the evidence of previous analysis and confirms how the directionality of the problem is a relevant variable.

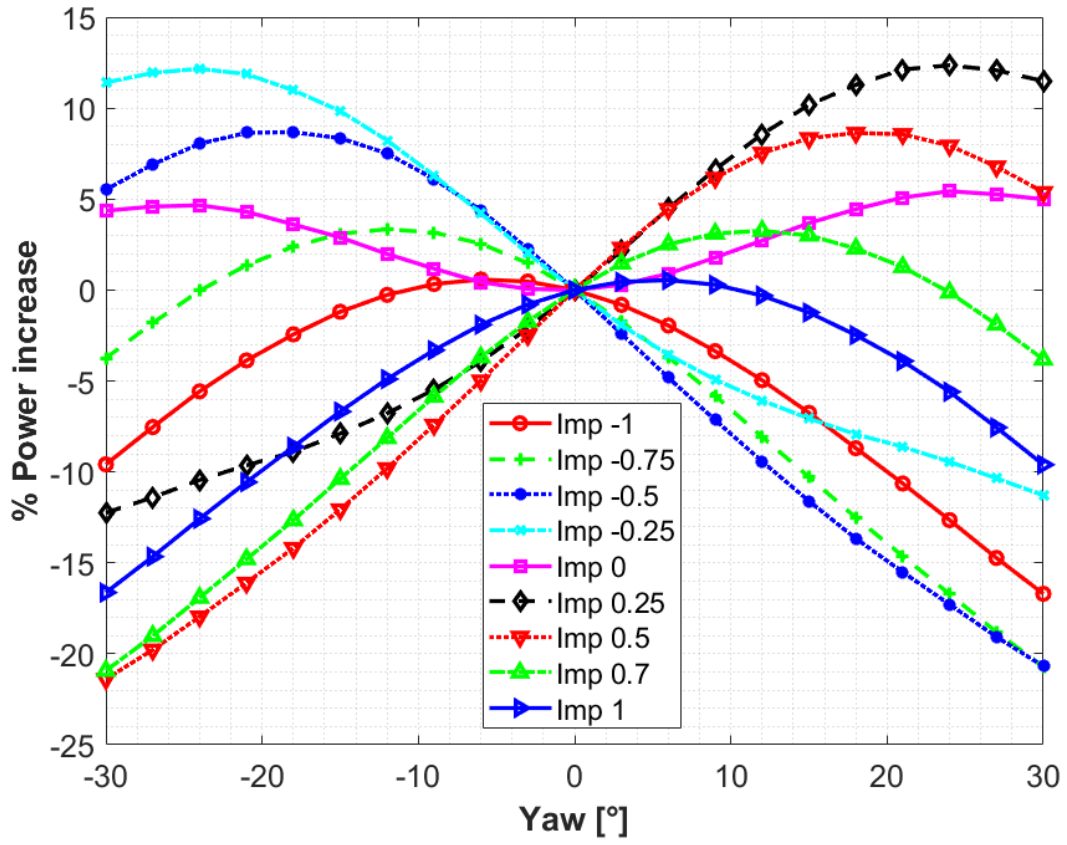

Figure 5.5: Parametric power curve over Impingement, Wind speed 11.4 m/s Offset 5 D TI 0.06

When looking at the constrained curve fig. 5.6 the same trends highlighted for the baseline case are found. The asymmetry of the curve is reflected once more in the uneven scaling of the graph, with the positive side of the yaw axis achieving better results than the left

side.

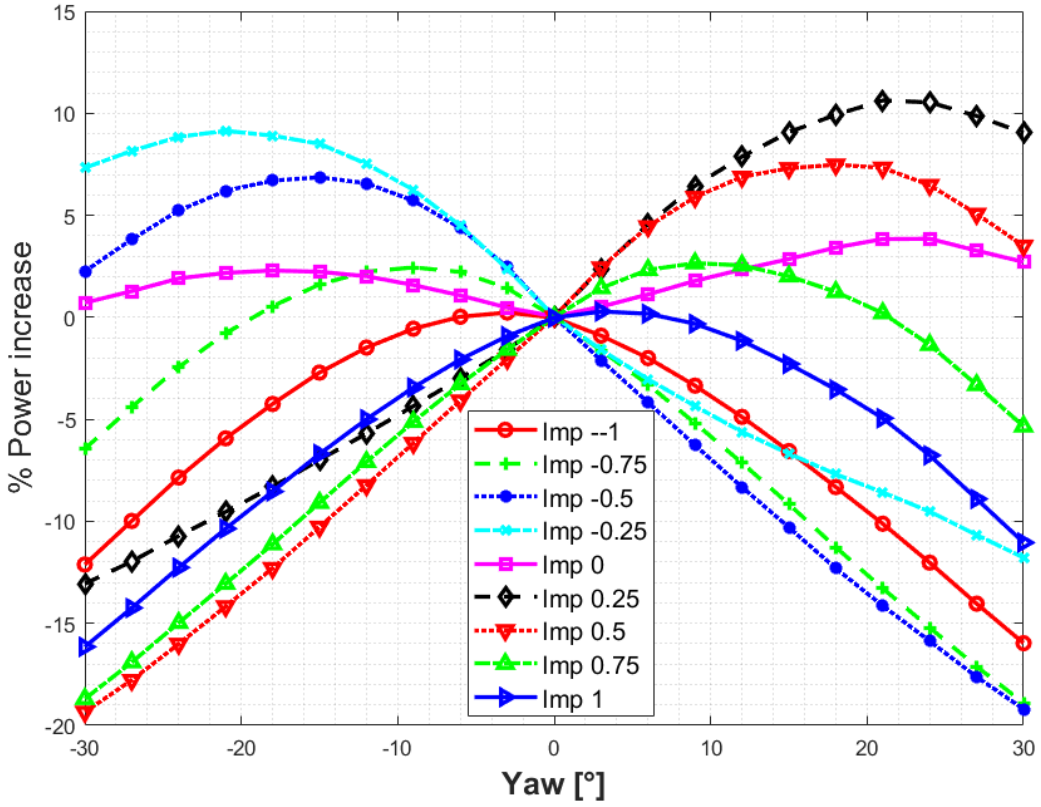

Figure 5.6: Constrained parametric power curve over Impingement, Wind speed 11.4 m/s Offset 5 D TI 0.06

Offset as a parameter is relevant because it is one of the specific proprieties of a given wind farm. Understanding the behavior of this control strategy depending on the offset between the turbines can help understand if this solution is a good option for a specific site. Figure 5.7 contains the power curve parameterized for the offset between the two machines. In this case, the control strategy's effectiveness increases with the distance between the machines. So much so that for Offset = 3D, the optimal result is for 0 yaw. This is an expected result as the closer the turbines are to each other, the sorter is the wake deflection for the same yaw angle. In this case this phenomenon is so relevant that the power lost by steering the first turbine is not recouped by the second one and yawing the first machine is actually a performance decrease. When the distance between the turbines increases, on the other hand, the wake steering control strategy performs very well and improves up until the 7D mark, when the maximum starts decreasing. The reason for this is that the graph shows the percentage power increase; therefore, it

measures the improvement over the uncontrolled case. At 7D, the farm is very close to expressing its full power output therefore, it makes sense seeing that the control strategy starts producing fewer improvements. By comparing the curves from 5 to 7 D it is also possible to see that the optimal value of yaw gets lower every time; this is due to the mechanism explained before, where the wake moves further for the same yaw angle if the offset is greater.

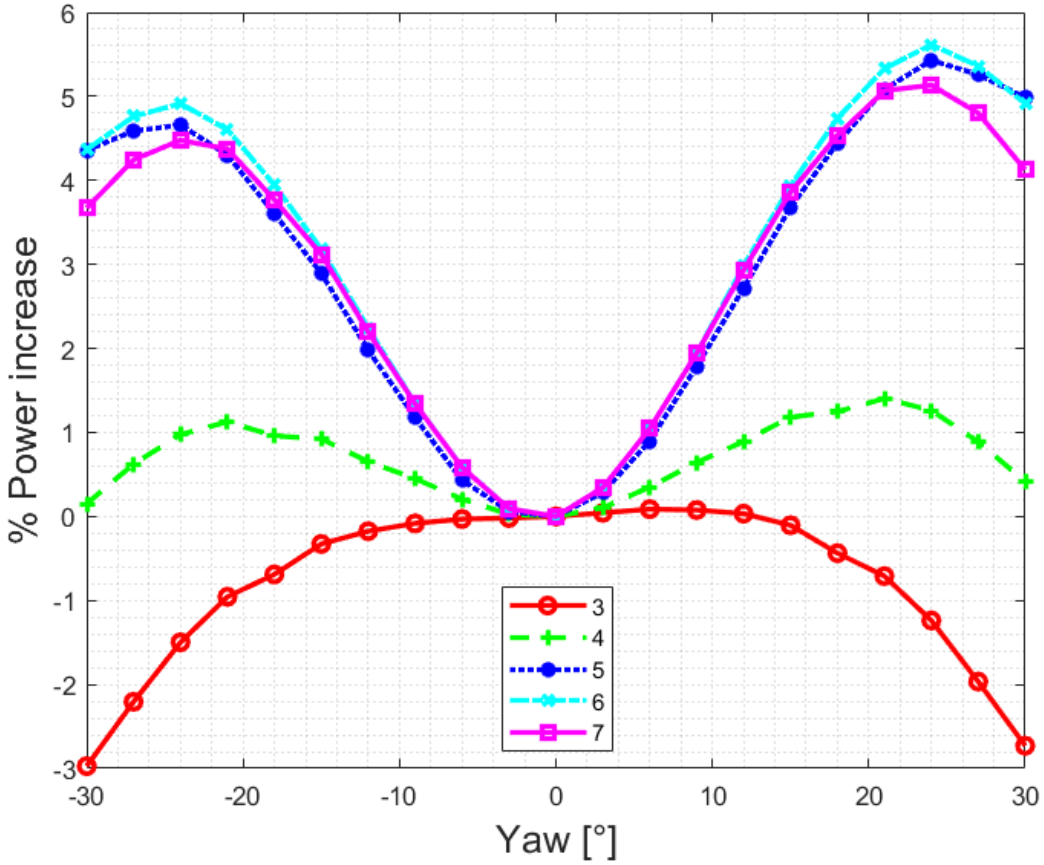

Figure 5.7: Parametric power curve over Offset, Wind speed 11.4 m/s Impingement 0 D TI 0.06

The constrained power curve is reported in fig. 5.8, this graph shows that when constraints are taken into account, once again the power curve becomes more asymmetric favoring the right side of the graph. A, perhaps, the less expected result is found near the 0 yaw line where, for the neighboring negative values, the 3 D case performs better than the others. This unexpected behavior prompts deeper research of those conditions carried on in the following subsection.

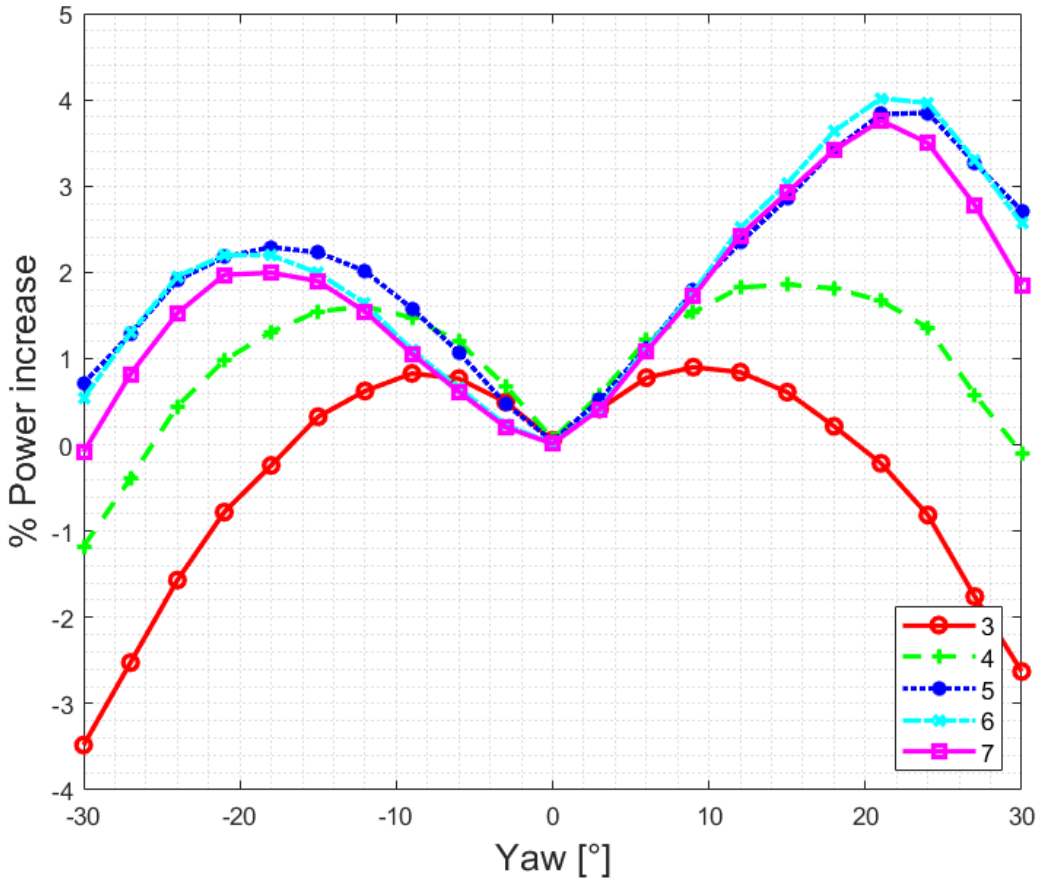

Figure 5.8: Constrained parametric power curve over Offset, Wind speed 11.4 m/s Impingement 0 TI 0.06

Figure 5.9 depicts the parametric analysis for the turbulence intensity. The meaning of this parameter suggests that the power production increases with the intensity of turbulence, this is due to the fact that the wake recovers energy quicker when the flow is turbulent. In terms of wake steering, this phenomenon means that although the total power production benefits from higher levels of turbulence, the effectiveness of the steering is reduced. In fact, since the wake recovers a large amount of energy in a shorter distance by the time this flow reaches the turbine at the back it does not have a big impact on how much it impinges on it as its velocity is closer to the one of the flow. This is true to the point that more energy is lost through the steering of the first machine than what is recovered by the back one.

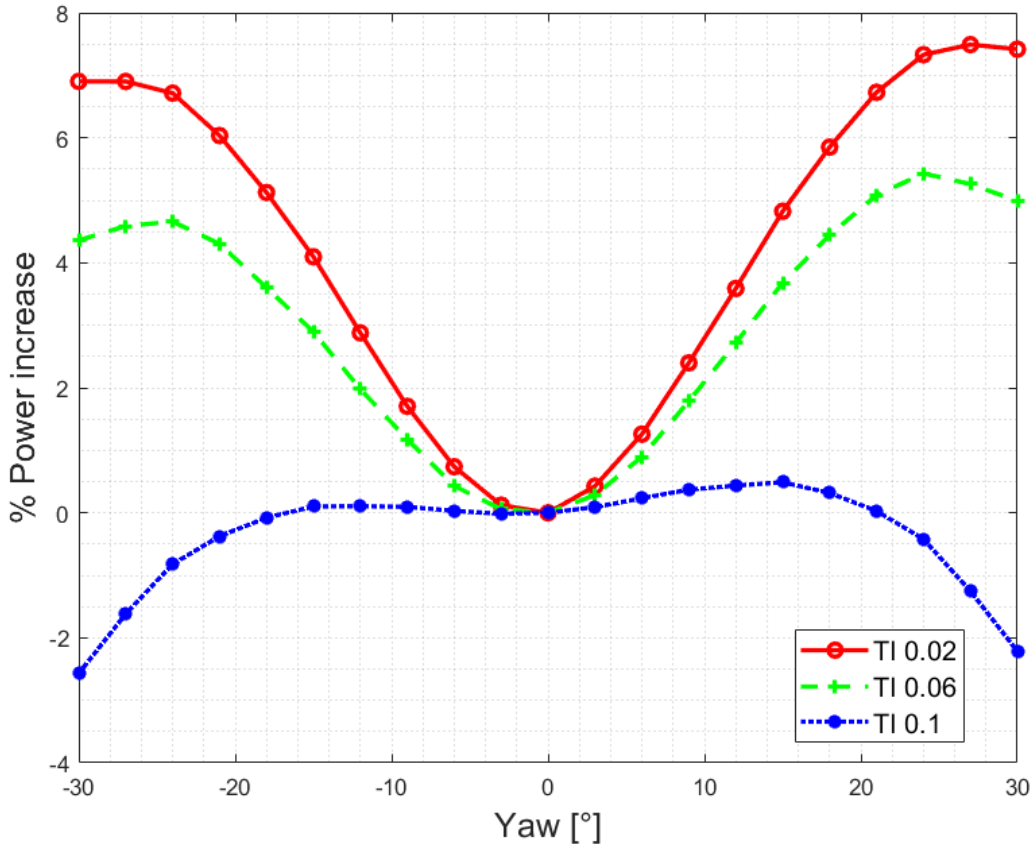

Figure 5.9: Parametric power curve over Turbulence Intensity, Wind speed 11.4 m/s Impingement 0 Offset 5D

The application of the constraint curve to this case is limited to projecting asymmetrically the yaw-only curve and doesn't change the conclusion extrapolated by the first analysis, as seen in fig. 5.10. What is notable is how small the power increment is for the case with TI=0.1, this suggests that in such conditions implementing an active wake redirection technique is not worth it; to find a definitive answer to this is necessary to look into the problem with different tools.

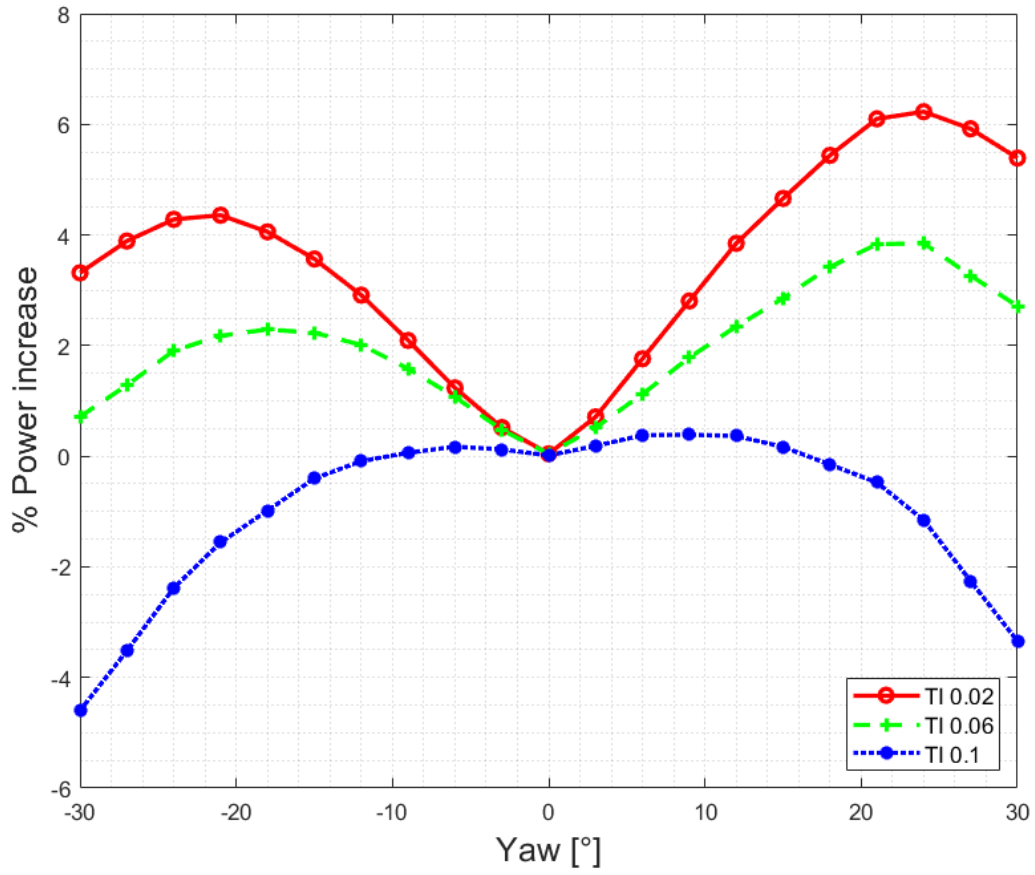

Figure 5.10: Constrained parametric power curve over Turbulence Intensity, Wind speed 11.4 m/s Impingement 0 Offset 5D

The parametric analysis for the wind speed is one of the most information-filled parts of this section and requires a bit of introduction to be properly explained. The key aspect to keep in mind while dealing with this topic is the power curve of a wind turbine. The power produced is defined as follows:

$$P = \frac{1}{2}\rho A C p V^3 \tag{5.2}$$

Where ρ is the air density, A is the area of the rotor, Cp is the power coefficient and V the wind speed. A typical power curve is depicted in fig. 5.11 and is constituted of three regions:

1. the startup region: the machine is off, and it is comprised of the space between wind speed = 0 and the cut in velocity

2. the cubic region: the machine is working at constant TSR and Cp is constant at its maximum value, this is the region between the cut-in speed and the rated speed. In this region, the power grows cubically as suggested by the exponent of V in eq. (5.2)
3. the above-rated region: the machine operates constantly at its rated power, this is achieved by controlling through the pitch actuators the value of Cp to compensate for the increase in wind speed. This region covers the field between the rated speed and the cutout speed.

When a turbine is steered the rotor is impinged perpendicularly only by a fraction of the total wind flow: only the normal component with respect to the rotor plane. This means that, for a given wind speed, when the machine yaws it is as if the wind is slower and in the graph this means moving on the power curve from right to left. On the other hand, steering the first turbine allows the back one to see a more intense wind, this in the graph is equivalent to a shift from left to right.

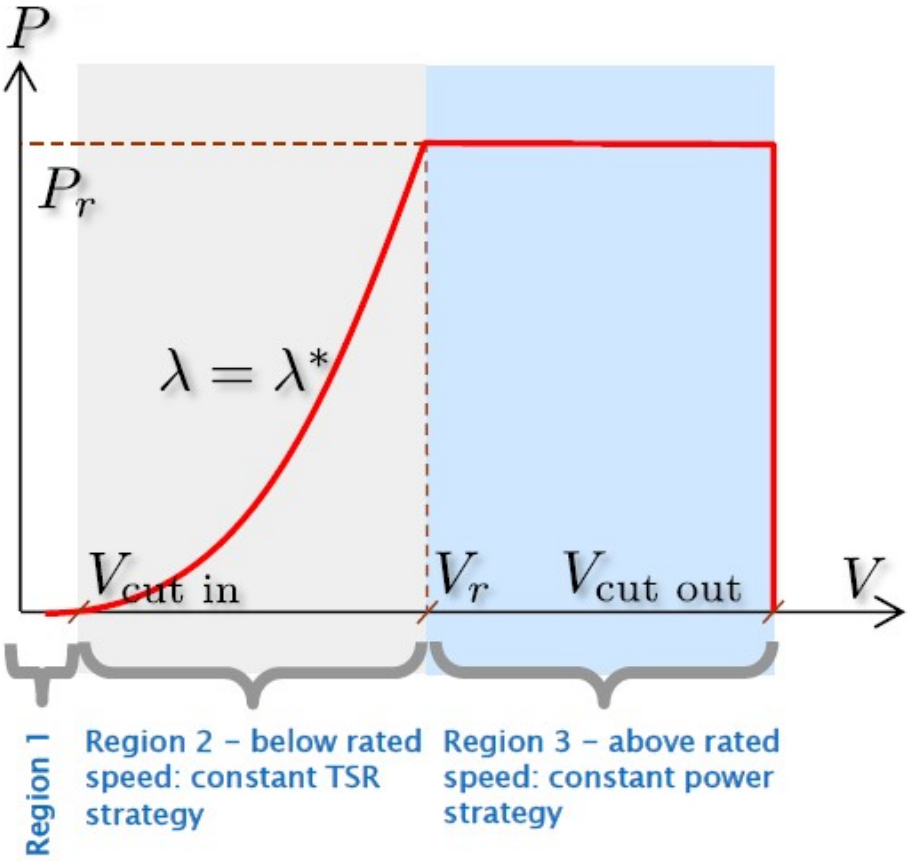

Figure 5.11: The power curve of a generic wind turbine. Credits A. Croce [18]

With this in mind it is possible to give a complete explanation of fig. 5.12. All the wind

velocities below V_{rated} show a similar increase in performance, in all three cases both machines operate in region 2, therefore it makes sense that the increase in percentage power produced is similar if not identical. Once V_{rated} is exceeded then things change, in fact the first machine is operating in region three therefore it is in the constant power region. While it is true that yawing the turbine may bring it back to region two, a significant amount of power that would be lost when yawing in region two is not lost in this case. This means that the power lost by the first turbine is less than in other cases while the power gained by the second is still significant as it is still operating in region two. This positive effect is, however, reduces as the wind speed increases because for a high enough value of wind speed, different for every configuration, turbine two also reaches region three effectively reaching the maximum power output of the farm.

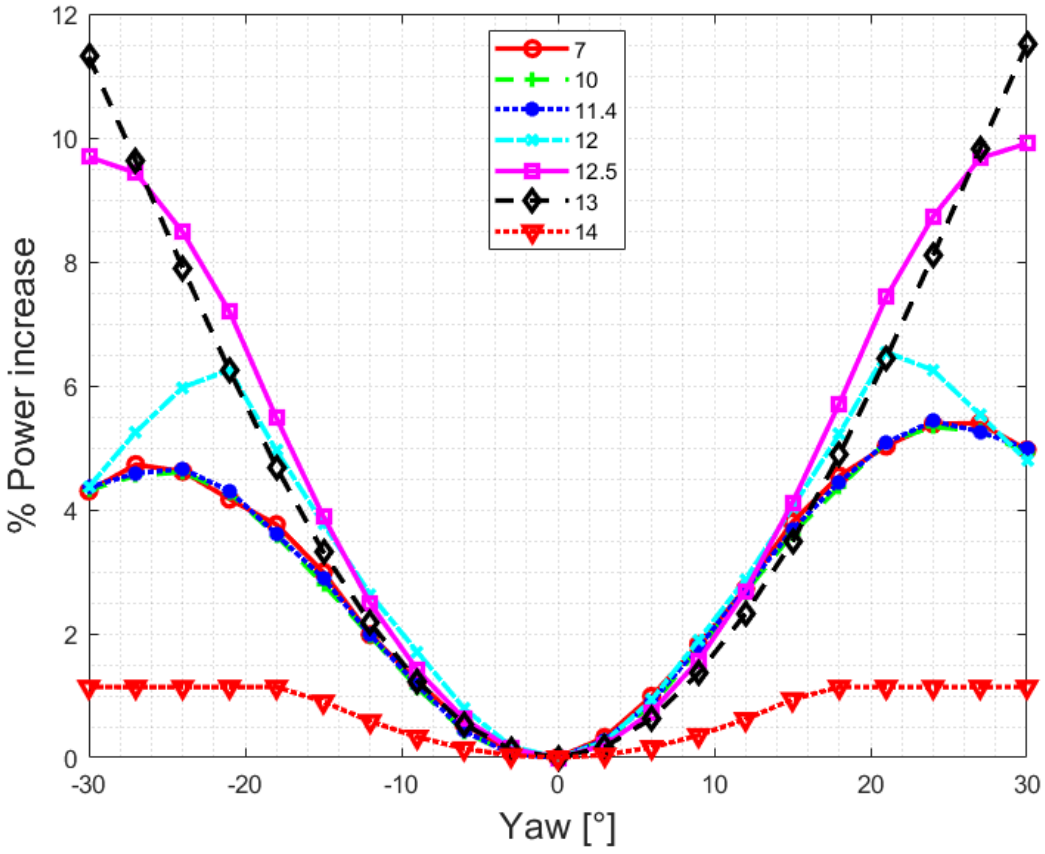

Figure 5.12: Parametric power curve over Wind Speed, TI 0.06 Impingement 0 Offset 5D

When considering the constrained problem things change, as seen in fig. 5.13. In fact in addition to the considerations made about the link between yaw and relative speed, the constrained problem to each yaw is associated with a minimum amount of derating. By definition derating the turbine lowers its maximum power output and scales down the

power curve as shown in fig. 3.4. This means that the benefits of operating in region 3, while still present are muted partially by this phenomenon: yawing a tribune in region three does not hinder power production, derating it does. The best visual representation of this concept can be done by comparing the 14 m/s curves for the unconstrained and constrained graphs. While in the unconstrained the power curve increases up to saturation and then becomes flat for the rest of the graph, if the derating becomes part of the problem, the opposite is true: the more the turbine is yawed the more it is derated and the more power is lost. This is relevant to the point that the optimal condition for the constrained problem is in 0 yaw 0 derating.

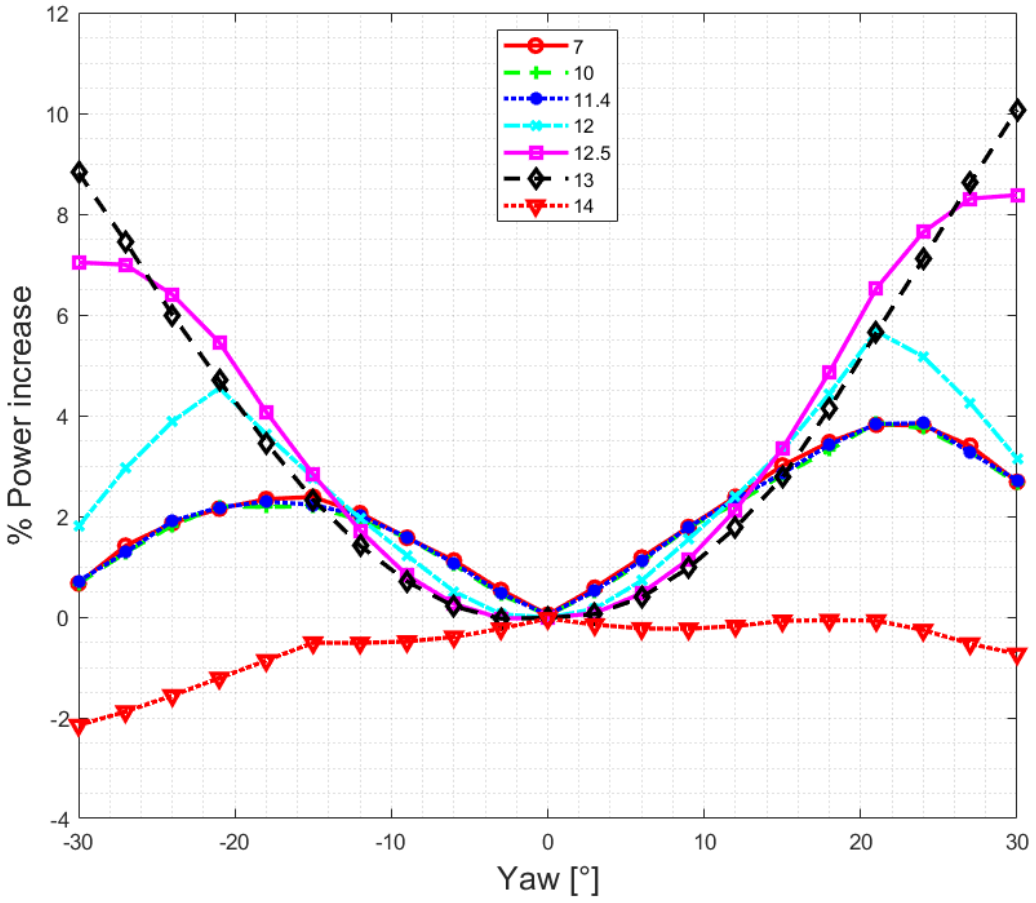

Figure 5.13: Constrained parametric power curve over Wind Speed, TI 0.06 Impingement 0 Offset 5D

5.2.3. Other cases of interest

One particularly interesting situation is where the machines are close to one another: offset = 3D. Under this situation the power curve for, the yaw-only strategy, is depicted in fig. 5.14. In this figure are highlighted the optimization results obtained with the yaw-only strategy, in this case the optimal power production is recorded for a value of around 10 degrees of yaw. As opposed to most other cases analyzed, the optimization result of the yaw-only strategy is not the overall best one. Figure 5.15 shows the contour plot of the PPI surface for the same conditions, from this graph it is visible the presence of an absolute maximum located in '5°, 2.6%'. This point is compliant with the constraint curve and it is also not resting on it. The consequences of this are that the only strategy that is able to capture this point as the optimal solution is the constrained yaw+derating one. For this reason it becomes relevant establishing what key parameters influence this behaviour and if the suboptimal solution given by the other strategies is deemed an acceptable approximation. In order to gather theses important informations, other analytical tools are necessary and they will be applied in section 5.3.1.

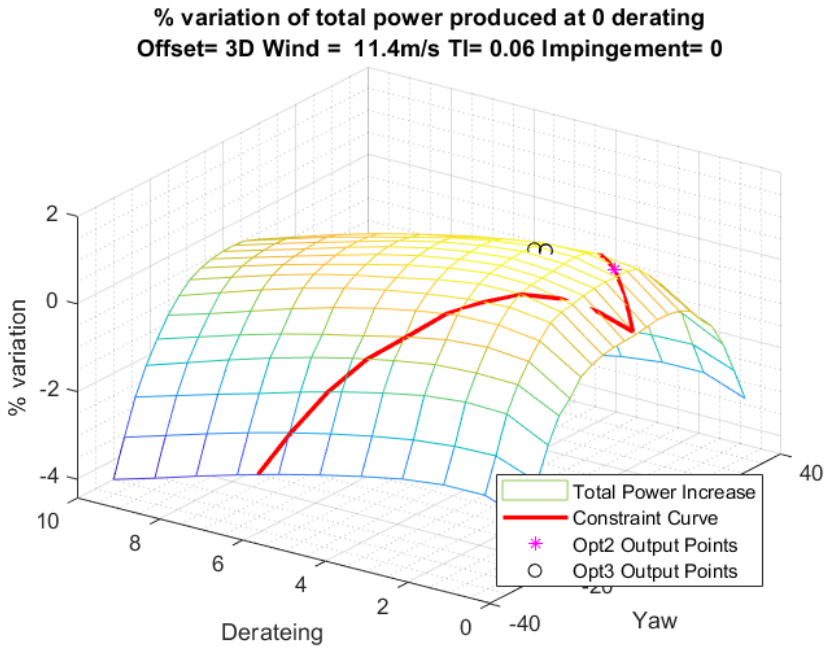

Figure 5.14: 3D surface graph of the PPI surface TI 0.06 Impingement 0 Offset 3D Wind 11.4 m/s

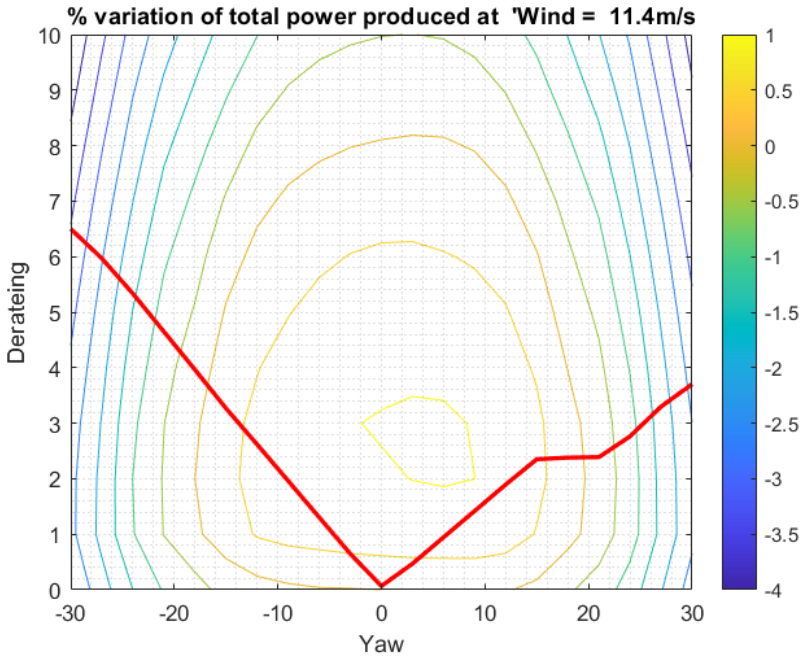

Figure 5.15: Contour plot of the PPI surface at TI 0.06 Impingement 0 Offset 3D Wind 11.4 m/s, with the constrained curve overlaid

Another case of particular interest is one for which the application of the constraint curve causes the optimal angle to shift for more than 20°. The case in question is: Offset 5D, Wind speed 14 m/s, Impingement 0.25 and TI 0.06. The yaw-only power curve is depicted in fig. 5.16, this graph has a much different look compared to the baseline one due to the overlap of the effect of many parameters changing. High wind speed, and the non-null impingement lead to a curve with an irregular profile showing three maximums and a very unpredictable shape. This is a great example of why it is necessity to use multiple starting guesses in order to make sure that the best possible conditions are found. By looking at the constrained power curve, depicted in fig. 5.17 it is possible to see an interesting phenomenon; here are reported both the optimization result of the suboptimal strategy, and the ones from the full-field constrained optimization. Contrary to most of the previous cases analyzed, applying the constraint curve drastically affects the shape of the power plot. This is due to the fact that the first turbine is well inside region three and the yaw redirection strategy is hardly of any effectiveness on the power production. In fact, the maximum power increment is only 1.5% and at an extreme angle of yaw, it is then clear that the effect of the additional derating necessary to fit the constraint curve for such an high angle can only lead to a power loss. This is confirmed by the fact that the optimal result is in 0 derating 0 yaw. What is also notable is how the constrained power has a very similar shape to the constraint curve itself, this is due to the power

surface being mostly flat with a constant negative slope in the direction of derating. This effectively shows that the behaviour of the farm at all yaw angles is the same as in zero and that, in these conditions, this strategy doesn't lead to any improvement. What has to be noted is how, although the optimal angle has shifted when comparing the optimal result of the yaw-only strategy and the one of the constrained problems, in correspondence to the new optimal value there is also a suboptimal solution in close proximity. Indeed since the optimization process is carried out starting from multiple different initial guesses, even when the absolute maximum shifts to another one, in all likelihood this result has been already mapped by one of the other guesses. This case is also a good representation of how the constraint curve can make it pointless to implement this hybrid strategy. In fact, while of only 1.5%, the yaw-only strategy showed an improvement in power production and, if the introduction of the constraints was not needed, it would have been worth steering the turbine. This leads to conclude that the introduction of the constraint compliance reduces the effective range of application of the hybrid control strategy.

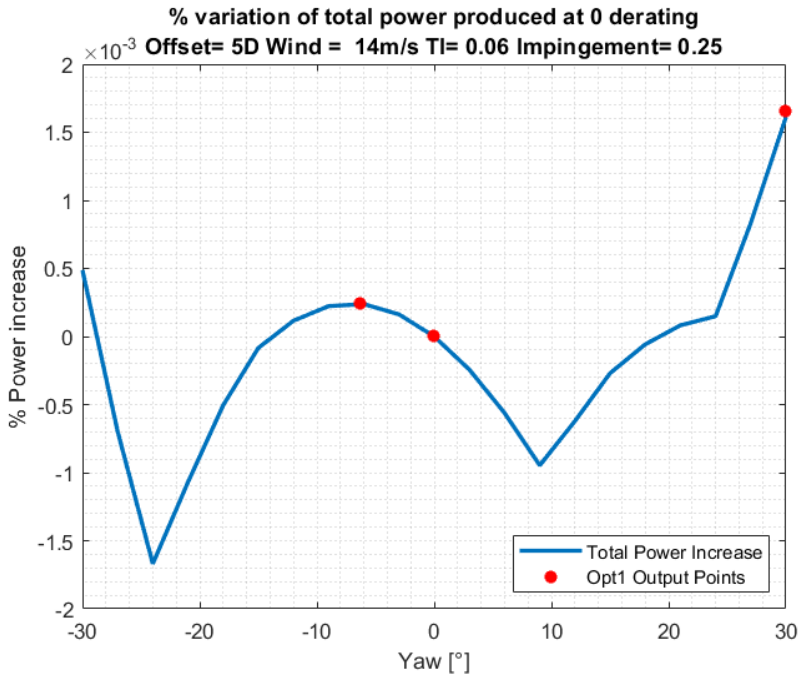

Figure 5.16: Yaw-only power curve for Offset 5D, Wind speed 14 m/s, Impingement 0.25 and TI 0.06.

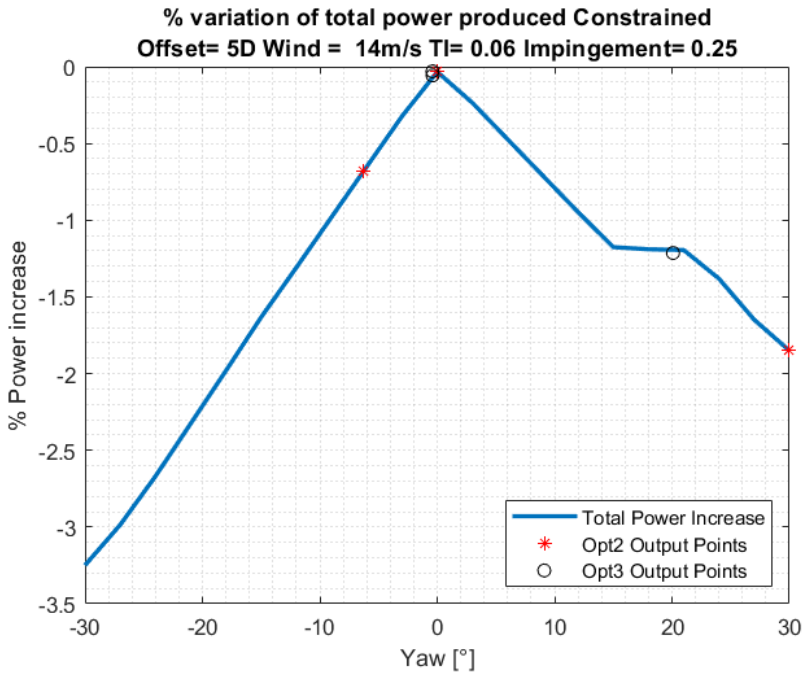

Figure 5.17: Constrained power curve for Offset 5D, Wind speed 14 m/s, Impingement 0.25 and TI 0.06.

5.3. Trend analysis for the optimal control

The scope of this section is to highlight trends and phenomena linked to the interaction between parameters. These curves will allow to figure out if the trends highlighted in the previous analysis are confirmed in a wider array of cases. In this section, optimal parametric curves will be used to discuss the effectiveness of the strategy over multiple conditions. Most of these graphs are built in the same way; a variable is chosen as the y-axis, and the options are:

- Yaw [°]
- Derating [%]
- PPI [%]
- Total Power Increase [KW]

The same is done for the x-axis variable with options:

- Offset [D]
- Turbulence Intensity []

- Wind Speed [m/s]
- Impingement []

The graph is then composed of the curve of the optimal value of the y-variable over the x-variable, all results are revered to the optimization result of the constrained yaw+derating problem. In many of the graphs present in this section also plotted some parametric curves, this means that the curves plotted are the values of the y variable over the x one but for a different value of one of the parameters. This kind of visualization strategy proves very effective because it allows plotting the effect of two variables changing on one plane. This section will also feature available powers plots, on these graphs the values of the best-performing optimization result are plotted over one of the x-variable. In order to not overcrowd this paper with graphs, this section will only be a subset of all the plots available as all the graphs amount to 64260 figures.

5.3.1. Offset

When speaking about this parameter the first that needs to be checked for consistency of the results is the behavior of the power output for lower levels of offset. This can be done by plotting the available power plot for the same conditions as the previous graphs, as well as looking into the yaw and derating trends for different wind speeds and impingement at offset = 3D. Figure 5.18 contains the aforementioned available power curve and the data confirms the trends highlighted in the previous sections. In fact, the enlarged picture, fig. 5.19, shows a zoom of the range between 3D and 4D, here the best performing strategy is by far the complete constrained yaw+derating followed by the suboptimal and the yaw-only. While this is without a doubt something that has a measurable impact on the total power output, it is also true that, if compared to the maximum power the farm could produce if the turbine did not interfere at all with one another, the increment is marginal. This is especially true if compared to the suboptimal strategy that delivers performances comparable by all means.

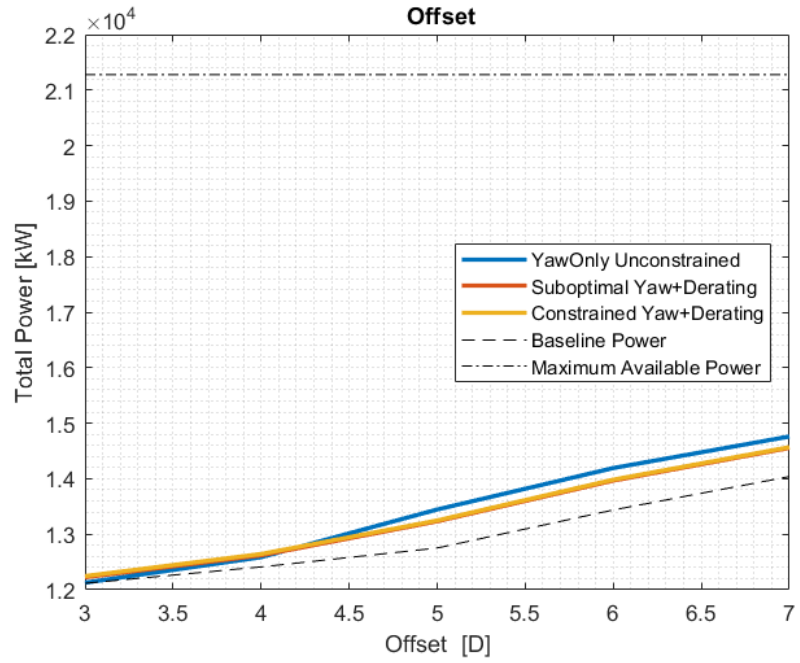

Figure 5.18: Available power curve for Wind speed 11.4 m/s, Ti 0.06 and impingement 0 with offset as variable

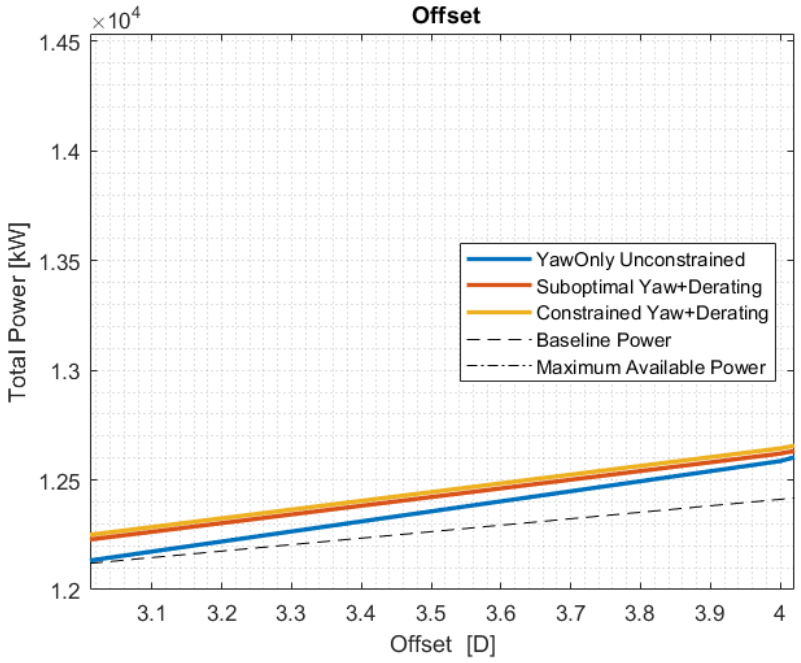

Figure 5.19: Available power curve for Wind speed 11.4 m/s, Ti 0.06 and impingement 0 with offset as variable (zoomed).

To now investigate if the change of other parameters interferes with this phenomenon,

the graph in fig. 5.20 shows the trend for yaw and fig. 5.21 the trend for derating as wind speeds and impingement change. In particular fig. 5.20 is a plot of the yaw over the wind speed with baseline conditions with parametric curves at different impingement. What is interesting here is how the optimal values are close to zero only for impingement 0 and ± 1 while the optimal derating for the same wind speed at impingement 0 is not 0. Of those two only the first one is representative of a situation where the axial induction control performs better than the yaw redirection. In fact, the cases for impingement ± 1 are representative of situations where the best angle for the yaw-only control is lower since the turbines are almost not interacting. For all other cases, a small difference in impingement is sufficient to make the yaw redirection the better performing strategy and behave like all other cases. Wind speed is also a factor to be mindful of, while almost all curves converge to the 0° for high winds, this is because the optimal solution is 0 yaw 0 derating for the reasons discussed above. The curve that is most of all important to monitor is the one for 0 derating that, for most values of wind speed, still shows the axial induction control as the superior method but with higher wind speeds this ceases to be true and the optimization shows the yaw redirection method as the preferred one.

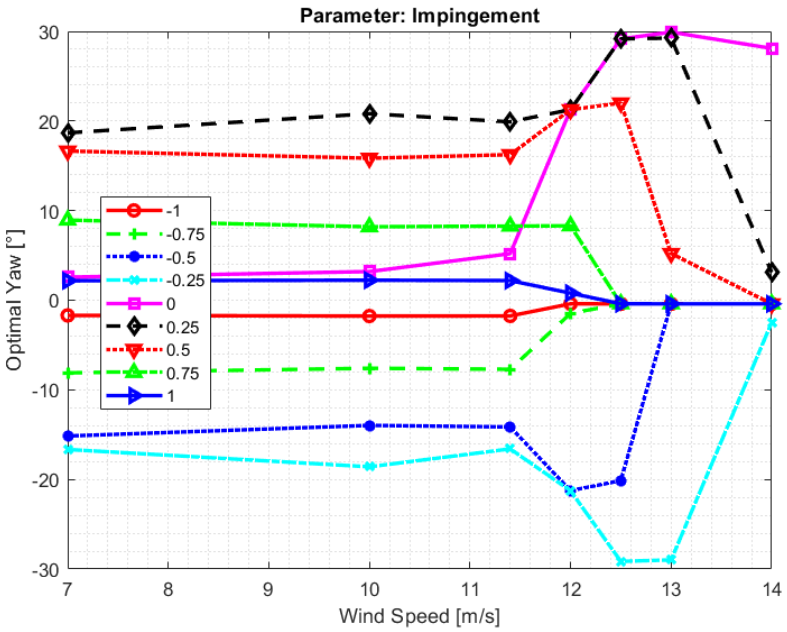

Figure 5.20: Optimal yaw curve for Offset 5D, and TI 0.06 with wind speed as variable and impingement as a parameter.

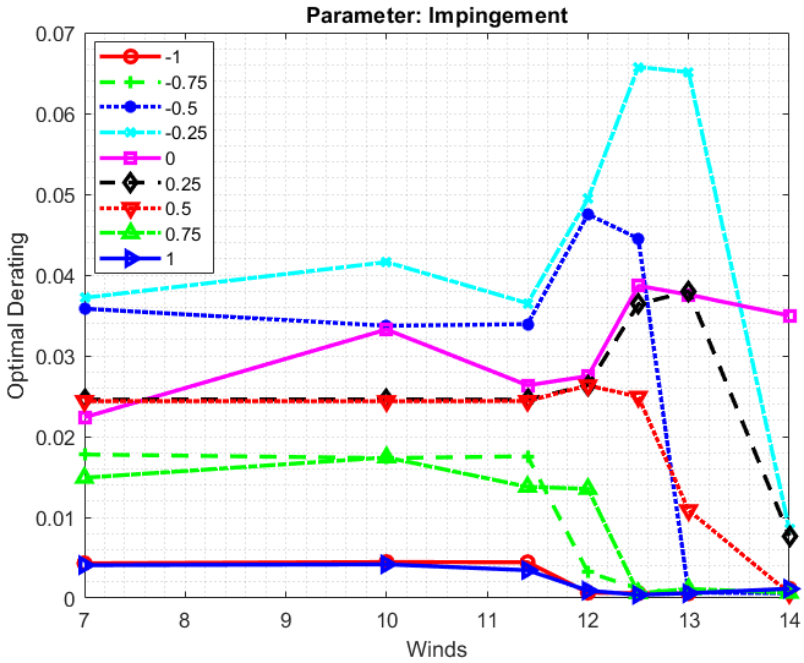

Figure 5.21: Optimal derating curve for Offset 5D, and TI 0.06 with wind speed as variable and impingement as a parameter.

In all of the cases viewed so far, the increase in offset is equivalent to an increase in power production, this is not the case for the parametric curves for impingement ± 1. Figure 5.22 is a plot whit impingement as the x-axis variable parameterized over the offset, this graph also shows the same trend as in the highlighted zones in fig. 5.23 the curves at lower offset deliver better power production. The explanation for this behavior is to be found in the shape of the wake, in fact, due to the fluid interactions with the surrounding air, the wake has a conical shape. This means that the further apart the turbines are the larger the wake will be in diameter, for the cases with unitary impingement this means that higher offsets lead to a larger portion of the rotor being impinged by the wake resulting in a performance loss. While this happens in all cases, in most of them both the large values of yaw and the energy that the wakes recovers thanks to the larger distance traveled outweigh this negative phenomenon making it hard to discern when looking at the power curves. The presence of such behavior is confirmed by fig. 5.24, here are plotted the parametric curves for TI over the offset at impingement one and wind speed 11.4 m/s. This graph shows that, in these conditions, an increment in turbulence level is associated to a power loss. This is due to the fact that the turbulence intensity determines, among other things, the shape of the wake and how fast it expands. FLORIS can help to visualize this phenomenon qualitatively, fig. 5.25 is the representation of the flow field for impingement 1, offset 7D

and TI 0.02, fig. 5.26 is the flow field for TI 0.1. While it is hard to gather to reach a quantitative analysis through this picture, it is clear how different the shape of the wake is and how this phenomenon influences the power produced. The figure for the lower TI shows a thinner but slower wake moving on a straight line, the other picture shows a faster but much wider wake interacting with the second turbine, this is exactly what leads to the phenomenon discussed above. With all of this being said it is important to keep in mind that the scale of this power reduction is very small compared to the total power produced, in fact for TI 0.1, impingement 1 and offset 7D at 11.4 m/s the difference in power with the same conditions at 3D of distance is only of 360 kW compared to the 19.5 MW produced.

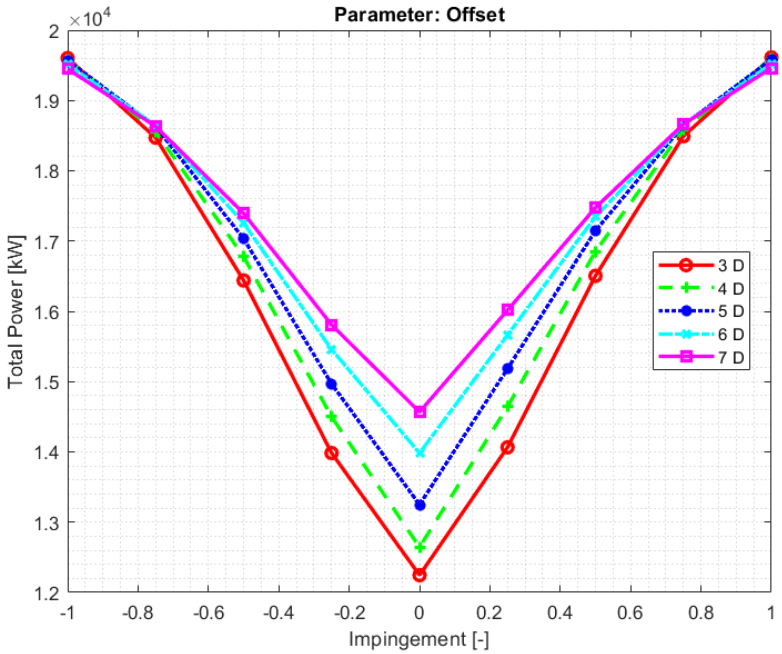

Figure 5.22: Total power curve for Wind speed 11.4 m/s, and TI 0.06 with Impingement as variable and offset as a parameter.

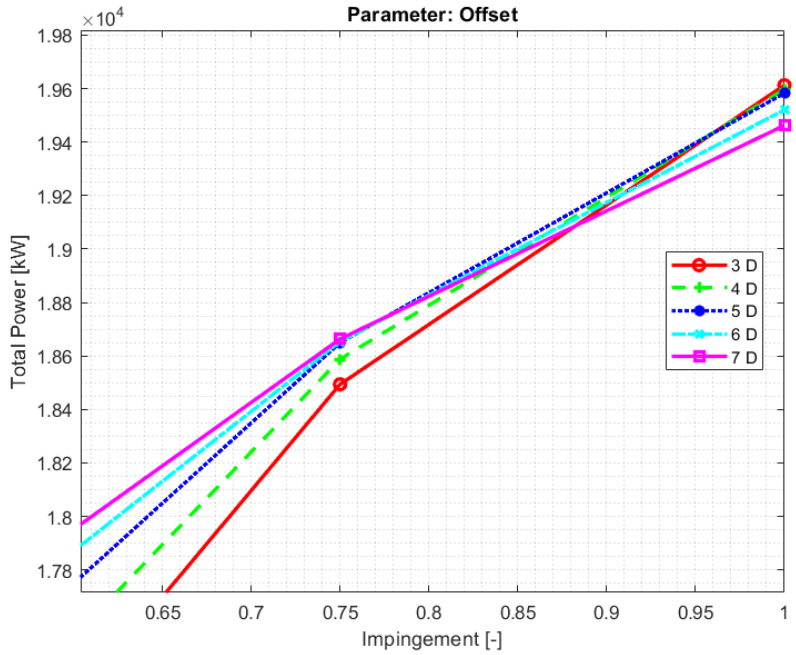

Figure 5.23: Total power curve for Wind speed 11.4 m/s, and TI 0.06 with Impingement as variable and offset as a parameter (zoom).

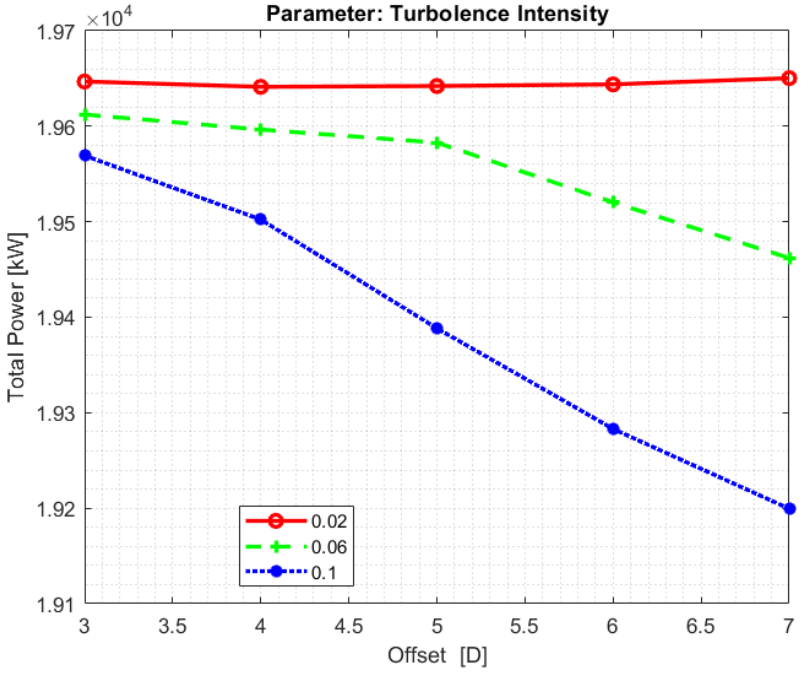

Figure 5.24: Total power curve for Wind speed 11.4 m/s, and impingement 1 with offset as variable and TI as a parameter.

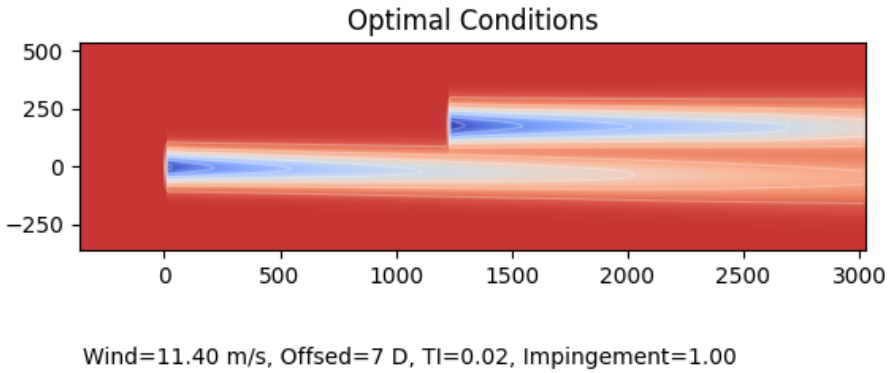

Figure 5.25: Representation of the flow field for impingement 1, offset 7D, wind speed 11.4 m/s and TI 0.02

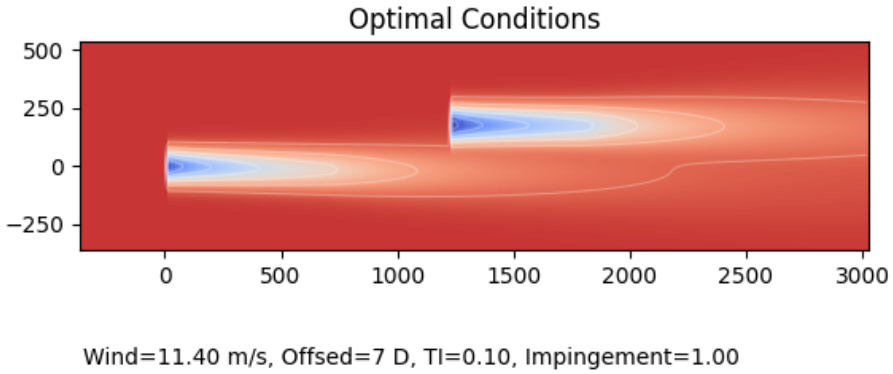

Figure 5.26: Representation of the flow field for impingement 1, offset 7D, wind speed 11.4 m/s and TI 0.1

5.3.2. Wind speed

Wind speed as a parameter is very significant as it is the dominant factor for power production. In addition to that finding the wind speed for which the control technique performs the best is crucial for understanding if a specific site is a good candidate for the application of this hybrid strategy. For this variable is best to look into the percentage power increase graphs as they are the most information-packed. Figure 5.27 represents the PPI curve parameterized over the offset. The first information to be extrapolated from this graph is about the scale of the PPI. While in other cases mentioned before the scale of the improvement reached values of 10 or even 15 % improvements, in this case most of the curves are between 0 and 5 %. This means that for the given baseline conditions there is little room for improvement at all wind speeds, all except for the values around

13 m/s. This wind speed range is the one discussed above where the first turbine enters region 3 and is saturated while the second one is still in region 2. As predicted, when the wind speed increases even more the farm reaches saturation, the control strategy is not needed, and the PPI drops to 0. In this region where the strategy is most effective the improvement is close to 15% for all the curves, to evaluate this, it is important to remember that in this conditions the farm is close to its maximum power output, therefore the improvement in total power is not negligible.

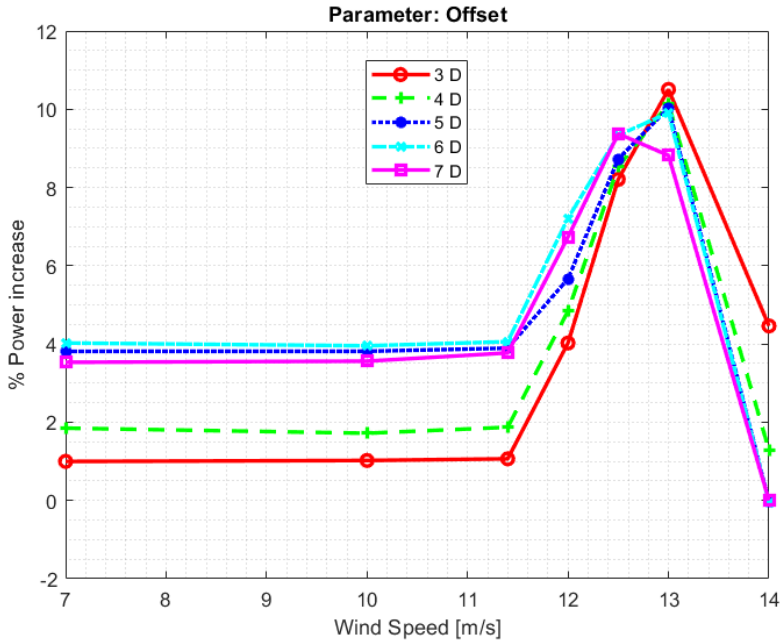

Figure 5.27: PPI curve for TI 0.06, and impingement 0 with wind speed as a variable and offset as a parameter.

The question that remains to be answered is if there are any factors that influence at what value of wind speed this phenomenon happens other than the V_{rated} of the farm. Figure 5.27 confirms that offset influences this phenomenon marginally, fig. 5.28 contains the parametric curves for TI. This graph also confirms that the speed of maximum effectiveness is the same regardless of the turbulence level. At last, fig. 5.30 shows the parametric curves for impingement. Here the situation is different and it is possible to see that different levels of impingement lead to a different maximum efficiency speed. First of all it is notable how for impingement = ± 1 and ± 0.75 the spike in power production is not present. This is due to the fact that in these conditions the second turbine is already almost out of the wake and the control system is not very effective. This is confirmed by fig. 5.29 that depicts the available power curves for imp 1 at $Vrated$, in these conditions even the unconstrained strategy does not grant major performance benefits . Here it is

clear that the control system has very little room for improvement, and therefore it is not very effective. Turning back the attention to fig. 5.30, for all the other curves the spike is present and happens at lower wind speeds for ±0.5, higher for ±0.25 and lastly at its highest for impingement 0. By definition the lowest possible point for this spike to take place is V_{rated}, because the first turbine has to be operating in region 3, with this in mind it makes sense that when the turbine at the back is impinged by less wake it reaches better performances faster. This is good news as in most sites it is more likely to operate at winds closer to the rated velocity rather than closer to the cutout speed.

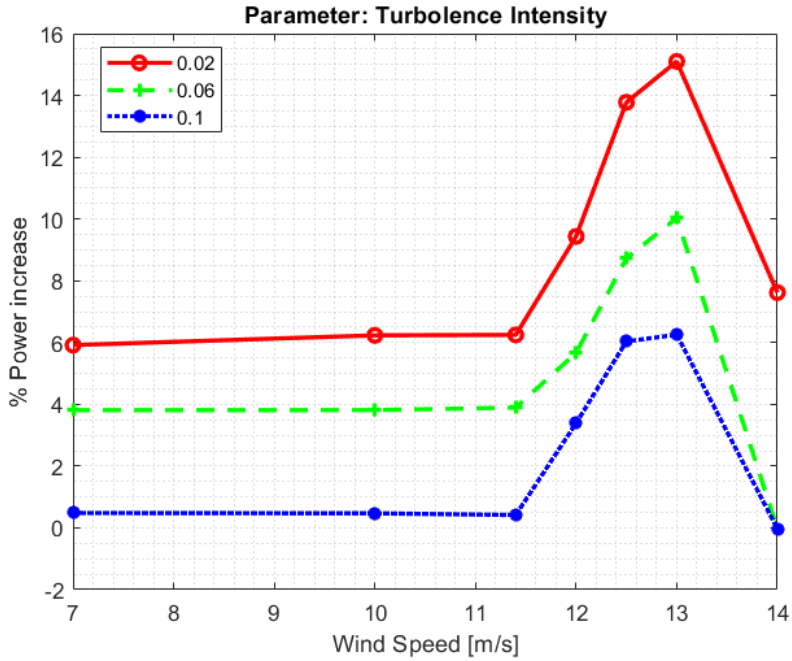

Figure 5.28: PPI curve for offset 5D, and impingement 0 with wind speed as a variable and TI as a parameter.

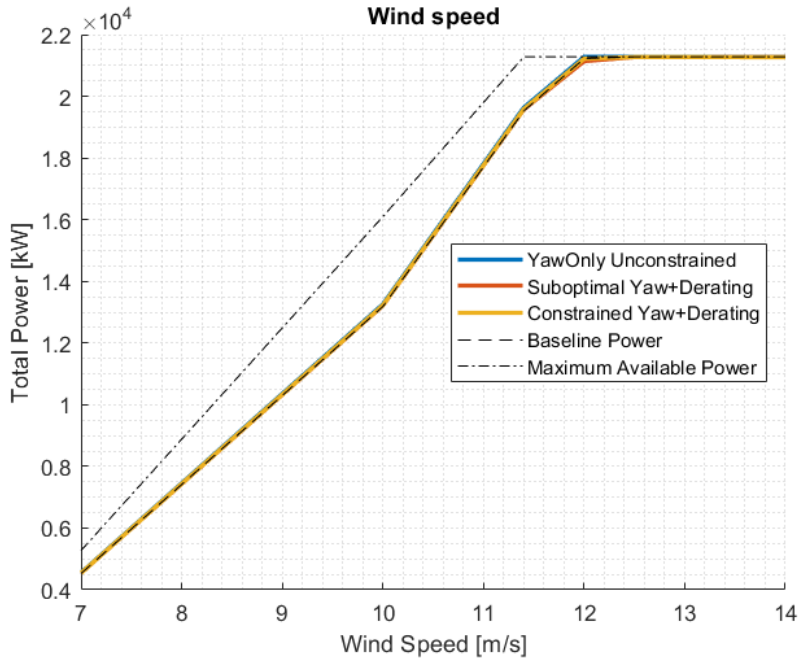

Figure 5.29: Available power curve for TI 0.06, impingement 0, and offset 5D with wind speed as a variable.

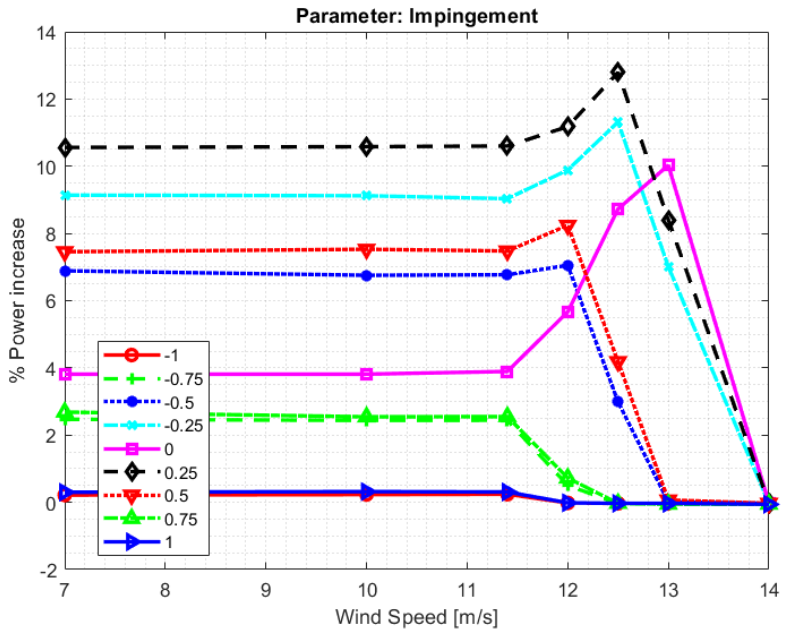

Figure 5.30: PPI curve for offset 5D, and TI 0.06 with wind speed as a variable and impingement as a parameter.

5.3.3. Impingement

This parameter has been mentioned multiple times because it interacts heavily with the active wake redirection strategy. In the previous sections it has been highlighted how it interfaces with the offset and how the effectiveness of the strategy is drastically different depending on the value of this parameter. In this section the objective will be to analyze the shape of the power graphs over the impingement. Clearly, the higher the impingement is the better performance is expected by the farm since, by definition, the second turbine is less exposed to the wake of the first. What is left to understand is how the effectiveness of the control system is influenced by impingement. The most useful tool to do so is the PPI graph with wind speed as its parameter. Figure 5.31 is exactly that, the result is fascinating as the shape of the curve changes with the wind speed. For all wind speeds of region 2 the shape is the same: there are two peaks in correspondence of ± 0.25, with the right one being slightly higher then the left one. This is an expected result based on the analysis in sec, it shows that the conditions of the highest efficiency are the ones for which the back turbine is not fully behind the front one. What is new about this graph is that it is possible to see a shift in the PPI curve as the wind speed gets higher. Once the first turbine is out for region 2, the margin for improvement is greater for impingement 0, this becomes more relevant the higher the wind speed gets up until saturation is reached. The scale of the peaks and their location is great news with regards to the effectiveness of the strategy as they mean that, in the worst condition possible for the farm, when the impingement is between -0.25 and +0.25, this control strategy performs the best leading to a total increase in power of up to 13 %.

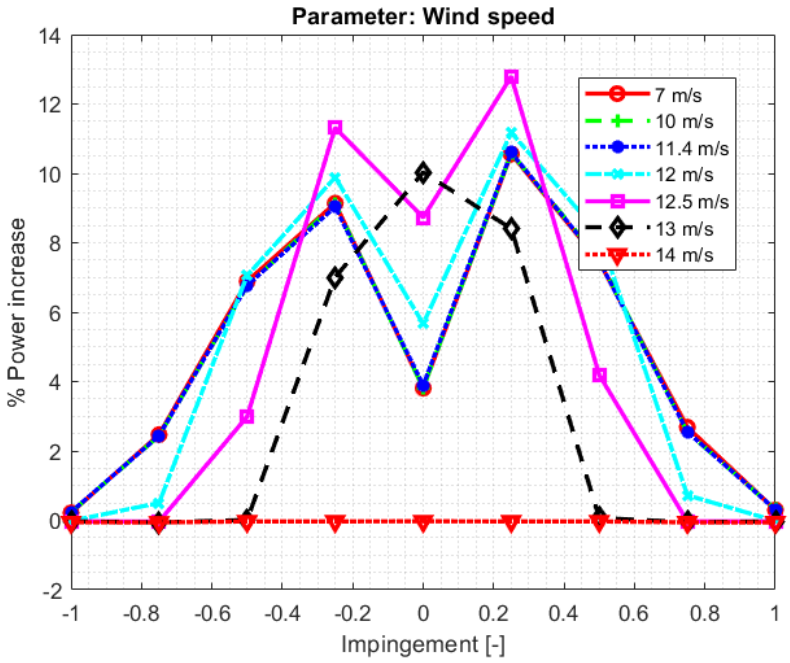

Figure 5.31: PPI curve for offset 5D, and TI 0.06 with impingement as a variable and wind speed as a parameter.

5.3.4. Turbulence Intensity

This parameter has the effect of improving the baseline and overall performances of the farm while also decreasing the effectiveness of the strategy. This dichotomy is consistent with the physical meaning of the parameter and the nature of the problem. The most peculiar aspect of this parameter is its contribution to the is how can change the effect that other parameters have on the farm in otherwise identical conditions. The most evident example of this is how a higher levels of turbulence favors the constrained optimization over the yaw-only one. While it is well established that for low offset, this phenomenon is present, if the turbulence level is high the optimal control strategy is the axial induction one for offsets up to 5D and wind speed up to 10 m/s.

5.4. Histograms

This section is focused on the analysis and comparison between the optimization results of the different strategies. The tool used for this comparison is histograms. This graphic tool allows visualize the difference between the optimizations across hundreds of simulations allowing us to draw conclusions that hold in the vast majority of cases. This section aims to answer all of the following questions:

- What is the expected power increase in a random situation: how effective is the control strategy in a generic situation
- What is the difference in terms of power production between the unconstrained yaw-only optimization and the other strategies: how much power is lost in order to satisfy the constraints
- What is the difference in power production between the suboptimal yaw+derating strategy and the constrained yaw+derating one: how much power is gained by setting up the complete optimization problem
- What is the difference in yaw between the yaw-only unconstrained and the constrained optimization: how close is the suboptimal solution to the optimal one

5.4.1. Effectiveness

The first step toward analyzing the result is looking at the performance of the optimization strategies across the whole spectrum of simulations. This is done in fig. 5.32, this picture represents through histograms the PPI registered in the 945 optimization solutions for all three strategies. What is most evident from this graph is that in over 50% of the cases analyzed there is only an improvement in power production between 0 and 2% in all cases. This means that even the most optimistic approach is only a marginal improvement over a farm without any active wake control. On the other hand over 40% of the simulations show an improvement grater then 2% with most of the results showing 5 to 10% more power produced. Overall the difference between the different strategies is pretty limited but there are some results that fit the expectations built by the previous analysis. The first and most evident is how the yaw only strategy produces across the board better results and is the strategy that has the least amount of elements in the bin corresponding to 0-1% increase. This was to be expected as this is usually the best case scenario. The fact that this strategy has anyways a large presence in the first bin can lead to concluding that a large sample of the cases considered show a minimal room for improvement. As expected the suboptimal strategy is the one that has the most assurances in the 0-1% bin and confirms the superiority of the full range optimization problem. Moving on to the higher PPI bins the only real noticeable trend is the superiority of the yaw only strategy with the other strategies producing extremely similar results. To better compare the strategy the next section will look at the difference in performance between the methods.

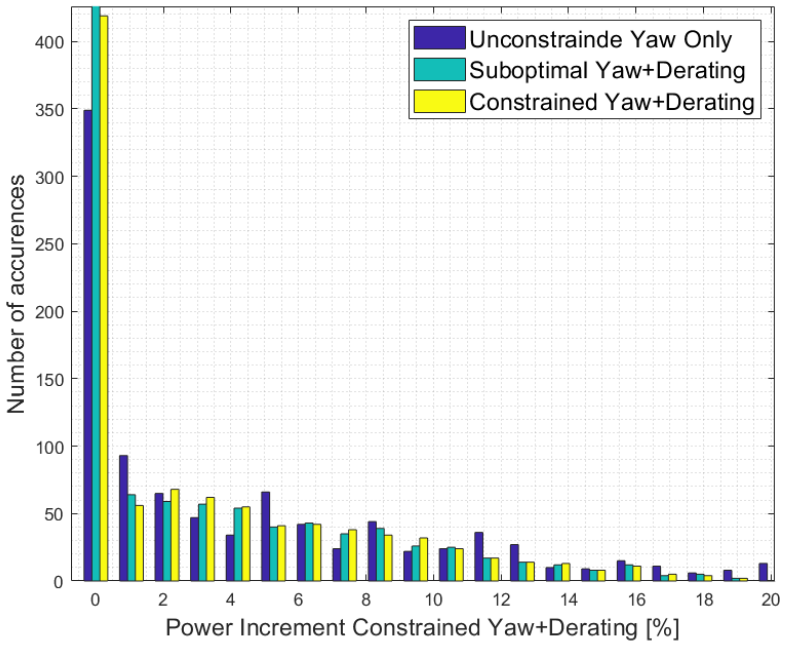

Figure 5.32: Histogram representation of the PPI of all three optimization strategies.

5.4.2. Power comparison

The first comparison analyzed is between Yaw-only unconstrained and Constrained yaw+derating strategies. By comparing the difference in PPI between the two strategies, it is possible to draw some conclusions on the potential of the hybrid approach. To interpret this histogram, it is essential to keep in mind what values it is presenting. The variable plotted is the difference in PPI computed over the entirety of the simulations. For each combination of parameters, the PPI of both strategies is computed and then subtracted as YawOnly-YawDer. By computing the results in this order, positive output values mean that the YawOnly strategy results in better power production. Conversely, negative values mean that constrained optimization has better power production. For the interpretation of the graph, the more concentrated the results are around 0%, the better the constrained strategy performs, and the higher the values are for positive percentages, the worse the strategy performs. fig. 5.33 depicts the histogram introduced above; in the graph 76.7% of the data is contained in the 0 to 2% range. This is very promising as this means that in the vast majority of cases, the farm's performance loss is limited to a fraction of the total improvement. It is also notable how there are two bins on the negative side of the graph and one centered in zero, these negative bins contain all the simulations for which the axial induction control outperformed the yaw redirection that have been extensively discussed before.

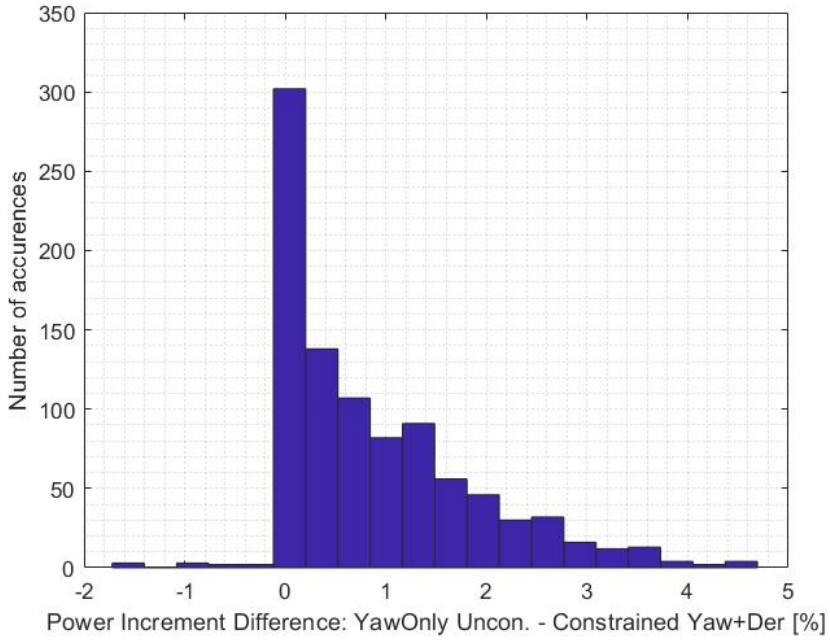

Figure 5.33: Histogram representation of the power difference between the unconstrained yaw-only strategy and the constrained yaw+derating

Figure 5.34 is depicts the comparison between strategies: unconstrained yaw only and the suboptimal yaw+derating. The first result from this histogram is that there are over 300 cases for which the power difference between the two strategies is null. By also considering fig. 5.32, it is clear that the conditions for which the PPI of both strategies are 0% when subtracted lead to a 0% difference found in fig. 5.34 meaning that the situation for which the yaw redirection is ineffective cannot be improved by implementing the suboptimal yaw+derating approach. Regarding the quantitative information given by the graph, it is notable how the bulk of the results fall under the 0% to 2% range. To be exact, out of the 945 simulations considered, the first bins up to 2% contain a total of 801 cases. The quota of simulations for which the PPI difference is less than 2% is 84.76%. Like in the comparison between yaw-only and the unconstrained yaw+derating, also in this case are found bins on the negative side of the graph. This means once again that there are situations for which the implementation of derting is beneficial in terms of power production.

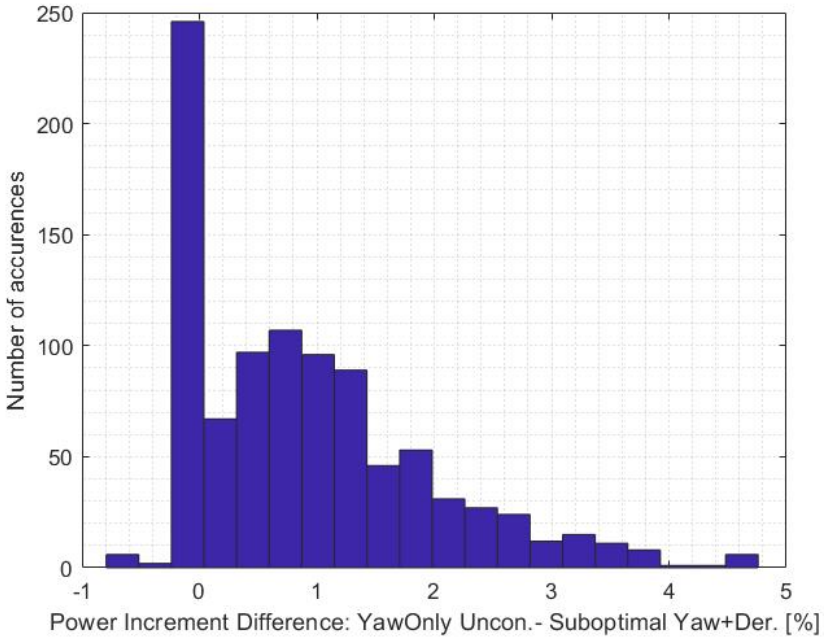

Figure 5.34: Histogram representation of the power difference between the unconstrained yaw-only strategy and the suboptimal yaw+derating

The histograms in fig. 5.35 contain the results of the comparison between the Suboptimal yaw+derating and the constrained yaw+derating optimization. The comparison is suboptimal PPI -optimal PPI; therefore, it is expected to show only non-positive values, however there is a small amount of positive occurrences, this is due to the tolerances set for the optimizer. These cases are a limited amount and most of them show a difference of less 0.1% therefore they can be allowed and considered as 0% difference. The results are fascinating as the totality of cases has less than 1% difference, and over the 90% of simulation show less than 0.4% of difference. This result shows a minimal decrease in performance if the more straightforward route is pursued. While this result shows little difference between the results of the two approaches, it is critical to remember that there needs to be a reason to justify, although minimal, a loss in the effectiveness of the strategy. While this approach could be promising to improve computational speeds when dealing with complex problems involving more turbines or more variables, this strategy has not been validated for those conditions. This result shows that, for the constraint curve considered, most of the optimal results for the unconstrained yaw-only strategy are also optimal for the constrained problem. In order to validate this strategy thoroughly, it should be tested with many different, reasonable constraint curves to ensure that the technique is viable no matter the shape of the latter.

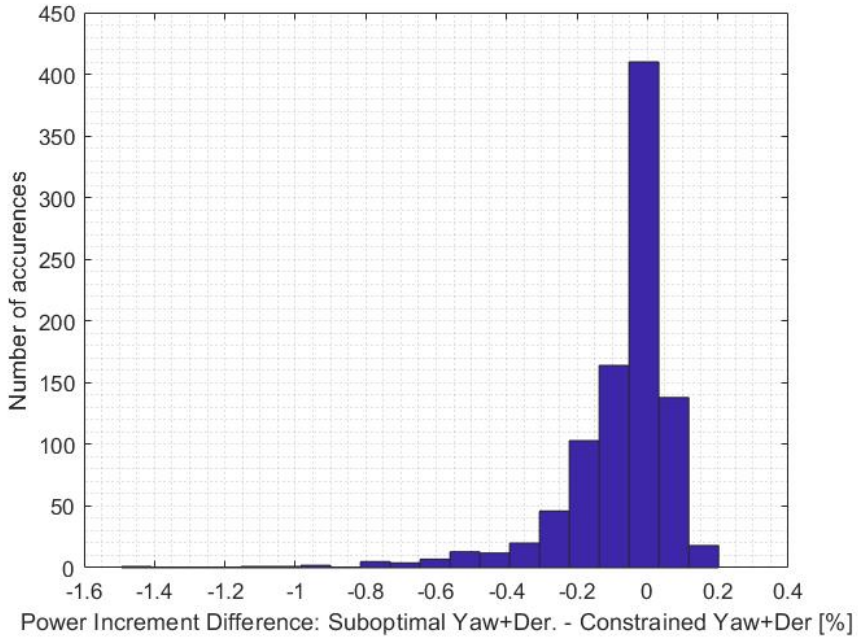

Figure 5.35: Histogram representation of the power difference between the constrained yaw+derating strategy and the suboptimal yaw+derating

5.4.3. Yaw Comparison

Figure 5.36 compares the difference in the optimal yaw registered over the whole database of simulations of all strategies. While it may be expected that the yaw angles of the suboptimal and the yaw-only strategies would coincide, this is not the case. As mentioned before, there are cases where the introduction of constraints effects the results by causing a shift in the optimal yaw value. This is evident by the significant population of the blue bins for high values of the yaw difference. While this is true, it is important to remember that multiple initial guesses have been used to find all the local optimal points, this is a great asset when the optimal yaw shifts because it is very likely that it moves from one absolute maximum to a local one that has been identified during the optimization procedure. This means that in most cases that show a large difference between the yaw-only solution and the constrained one there is a suboptimal solution close to the optimal. This is confirmed by the graph as there is a sensible increase in cases close to 0° of difference and the absence of cases with large differences.

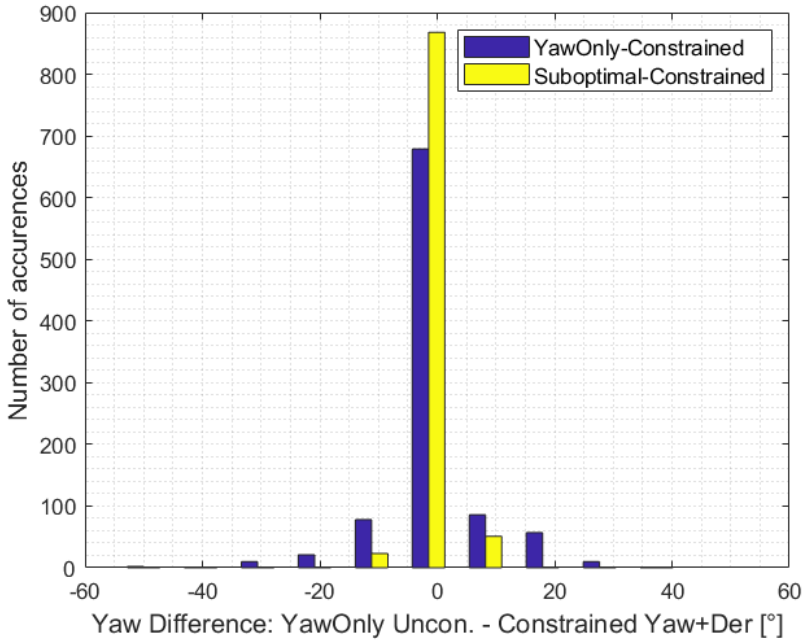

Figure 5.36: Histogram representation of yaw difference between the optimization strategies

5.5. Review of the results

The key concept to keep in mind while evaluating the results presented is that they are only a limited subset of the available data gathered from5 the simulations. In fact just from the tools implemented for the post-processing it is possible to plot 64260 different figures. Such a large sample is very hard to comprehend to its fullest potential, in fact the main problem in analyzing the results is their sheer amount. Since one of the goals of the thesis is highlighting trends among the changing parameters, it is necessary to define some baseline conditions and then compare the other results to it. While this approach is very functional to reach the aforementioned goal, it lacks a wider view of all the 945 possible combination that have been simulated. While it is possible that some trends present in the simulation output have not been spotted, the histograms have been used to find any outliers and grasp a deeper understanding of the conditions that led to those results. The parametric curves have proven to be the best tools to tackle the complexity of the problem and have provided a great overview of the connection between the different parameters. In this phase it must be noted that a large amount of the simulated condition led to a 0% PPI, this should prompt a deeper research in the field of application of this technique.

6 | Conclusions

Starting form the definition of the structural requirements of the wind turbine subject to the control strategy, it has been defined a set of optimization problems. The three techniques emerged form this process have been implemented through a optimization algorithm and tested in a computational environment. Thanks to FLORIS and the large degree of customization available it was possible to simulate 945 different conditions mapped by four different parameters. The data gathered through this process has been then post-processed through a custom software and the results have been presented in this paper. Note that, starting from the 945 simulation it is possible to produce 64260 plots, and clearly such a large number of figures can't fit in this paper and only the one deemed necessary to explain phenomena have been chosen to be a part of this thesis. The main findings of this paper can be summed up briefly in the list that follows:

- The operating conditions are a crucial factor for the effectiveness of the strategy. The cases for which this technique leads to meaningful improvements are a subset of the ones where this happens for unconstrained wake redirection.
- While this strategy features two optimization techniques simultaneously, they do not show a synergistic behavior: if one produces optimal results applying the other leads to power losses.
- In cases with a low offset between the turbines, the hybrid strategy outperforms the yaw redirection one because it can apply axial induction control to solve the problem.
- This strategy produces the best wind performance above the machine's rated speed. It leads to a significant increase in power production when the farm loses the most energy.
- This strategy is not very efficacious for extreme values of any parameters, both high and low. The best results are produced in conditions close to the medium of the parameter simulated.
- In the cases where the strategy is deployed (PPI$>$0.5%), the average power increase

is 6.5%.

- While still delivering lower performance than the optimal strategy, the suboptimal approximation averages a 0.069% power output difference compared to the optimal strategy. This makes this strategy a viable approximation.
- The constraint curve is an active variable in the problem, and its definition influences all the results. The one used for this thesis is the most conservative possible given the farm, and this should be considered when evaluating the results.

Based on this list of results it is possible to conclude that this strategy is a viable solution for already existing wind farms. It is undeniable that in a substantial amount of cases applying this technique delivers non-negligible improvements. In terms of applicability there is a lot of potential as the constraint curve can be computed for each situation and model every wind turbine already deployed. The absence of any structural upgrade or modification necessary is an excellent asset as it can keep the costs associated with applying this control strategy. It is also worth noting how closely the suboptimal strategy follows the optimal results. This is very important because it allows us to reduce the complexity of the problem and the number of variables involved making it more accessible to add complexity in other ways.

6.1. Future developments

Future development for this thesis includes but is not limited to the one listed in this section. The inclusion of multiple constraint curves is the first and most cited avenue for improvement that has been cited multiple times across the document. This curve actively determines the effect of the control strategy on the farm, and it is of great interest to research if a different curve can lead to a different conclusion about this control technique. Another point of interest is the fatigue analysis of a farm operating under this control law. While the structural analysis has been carried out for the steered turbine, the impact on the turbine at the back has not yet been researched. This study should be carried out both in terms of ultimate loads and in terms of fatigue loads. The most challenging part of conducting such research is modeling the wake correctly to reach scientifically relevant results. This is relevant because the wake is a notoriously turbulent flow that can lead to vibrations and fatigue problems. Last but not least is the introduction of more variables and more turbines. While this paper is meant to be a proof of concept, it is rare to find farms made by only two turbines in real-world applications. In order to reach results more closely related to a real scenario, more turbines should be considered, and it should be noted the possibility of the second turbine yawing as well. It is also possible to model

even more aspects of the environmental conditions; for example, the boundary layer can be included, as well as changes in density and many other variables.

Bibliography

[1] Gianluca Dadda. Impact of combinations of wind farm controllers on wind turbine loads. Master's thesis, Politecnico di Milano, Piazza Leonardo Milano, 04 2021.

[2] Croce A. Cacciola S. and Sartori L. Evaluation of the impact of active wake control techniques on ultimate loads for a 10mw wind turbine. 2021.

[3] European Council. Fit for 55, 2022.

[4] European Council. European green deal, 2022.

[5] Irena. Future of wind: Deployment, investment, technology, grid integration and socio-economic aspects (a global energy transformation paper)., 2019.

[6] European Council. Fit for 55 infographic, 2022.

[7] European Commission. A clean planet for all, 2018.

[8] Robert Rapier for Forbes. Why natural gas prices quadrupled in two years, 2022.

[9] Danish energy's agency. Denmark's energy islands, 2022.

[10] Tony Burton et al. Wind energy handbook, 2011.

[11] J.Å. Dahlberg and S.E. Thor. Power performance andwake effects in the closely spaced lillgrund offshore wind farm., 2009.

[12] P. Gebraad et al. A data-driven model for wind plant power optimization by yaw control, 2014.

[13] P. Fleming et al. Simulation comparison of wake mitigation control strategies for a two-turbine case, 2014.

[14] C. et al. Bak. The dtu 10-mw reference wind turbine, 2013.

[15] NREL. Floris, a brief tutorial, 2018.

[16] J. Schreiber et al. Verification and calibration of a reduced order wind farm model by wind tunnel experiments, 2017.

[17] Paul Fleming et al. Initial results from a field campaign of wake steering applied at a commercial wind farm: Part 1". in: Wind energy science discussions, 2019.

[18] Alessandro Croce. Slides form "progetto di generatori eolici", AA 2021-2022.

A | Appendix A

This chapter is dedicated to the explanation of the structure of the software and how to operate the scripts. As mentioned in the document, most of the scripts are run by MatLab, with python used as a "black box" to compute the power produced based on a series of input files. To understand the setup, it is necessary to familiarize with the input required by a FLORIS script to run. The input files are layered on two levels: the highest is a farm that defines the site-specific proprieties, like layout, TI, and many others, while also loading the turbine models from the turbine library. The turbine library is a folder present within the installation folder of the tool. It contains all the data of the turbines and, most importantly, all the power and force coefficients. This means that when the python script gets executed, it loads a farm that loads the turbines. By providing specifically formatted .txt files in a specific folder, the script can reinitialize the parameters that need to be simulated, and it outputs the power output of the turbines via its console. The console is red by the MatLab script that launched the FLORIS simulation completing the "black box" operation and linking some input parameters to power produced. This function is then used as the basis of the objective functions to be minimized by the solver with the necessary modifications for each optimization strategy. For each combination of parameters, all the strategies are run three times with different initial guesses and saved as a unique struct in a specific folder at the end of the process. Each output file contains the parameters of the simulation and, for each guess of each strategy, the optimal values of the variables and the power produced by both of the turbines. These output files can then be gathered in a database to be analyzed by the postprocessor. The process is summed up in fig. A.1.

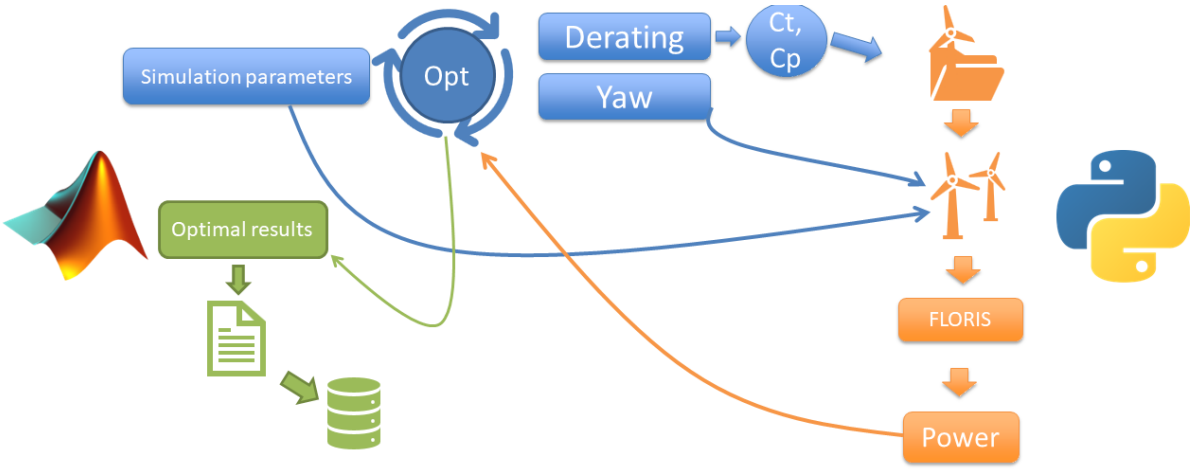

Figure A.1: Complete overview of the optimization process

The window that interfaces with the user is depicted in fig. A.2; from there, it is possible to choose the configuration to evaluate, thanks to the drop-down menus highlighted in the orange box. The two switches enable the user to choose what analysis has to be carried out. The one inside the blue box toggles whether or not the power curves for the single configuration get displayed, while the one in the green box is used to toggle the parametric analysis. It is also possible to produce the parametric power curves shown in the document from this window. Once the desired setting has been chosen, the button run starts the computation; this can take from one minute, for the standard power curves, up to several for the parametric ones depending on the number of parametric cases. The long computational time is because, to produce these results, the entire field of yaw angles and derating has to be computed for each combination of parameters. To help visualize the situation analyzed, this application also runs a dedicated FLORIS script that produces and saves a figure of the farm in the optimal condition found during the optimization for the parameters chosen.

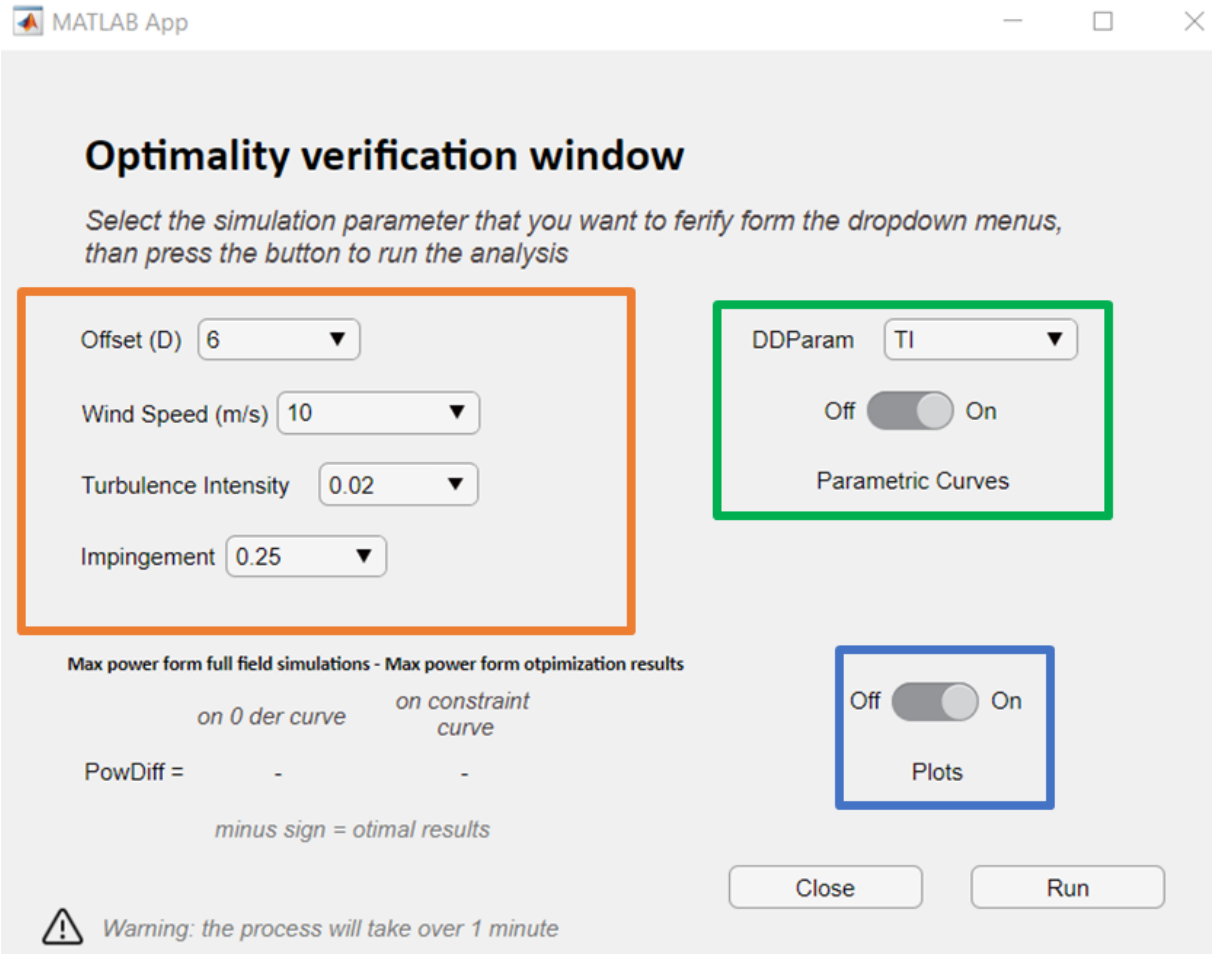

Figure A.2: Screenshot of the optimality verification app whit highlighted fields

The following figures are an example of the output produced by hitting the run button whit the setting of fig. A.2. Figure A.3 and fig. A.4 are the parametric curves, fig. A.5 is the contour plot and fig. A.6 contains the plots of the simulated conditions. Figure A.7 is a representation of the simulated condition with FLORIS.

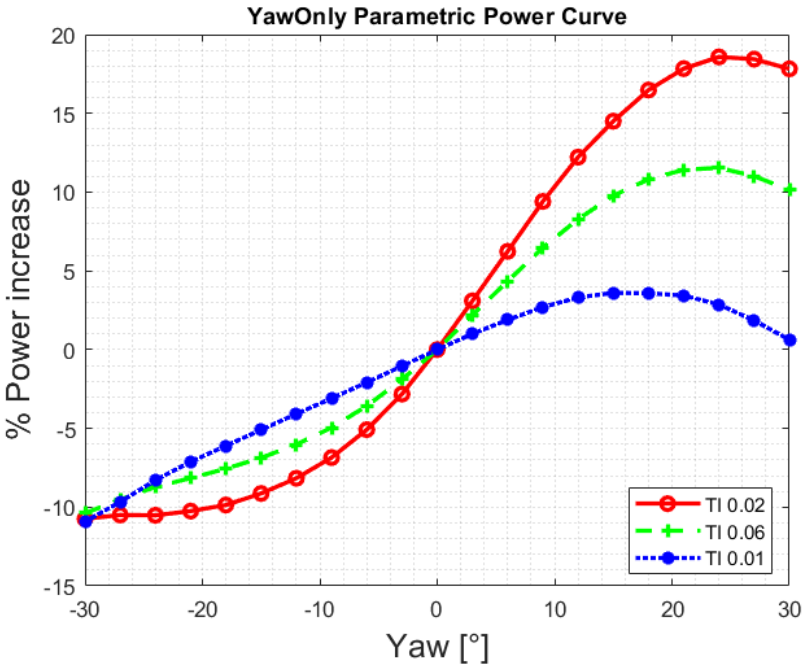

Figure A.3: Yaw only parametric power curve example

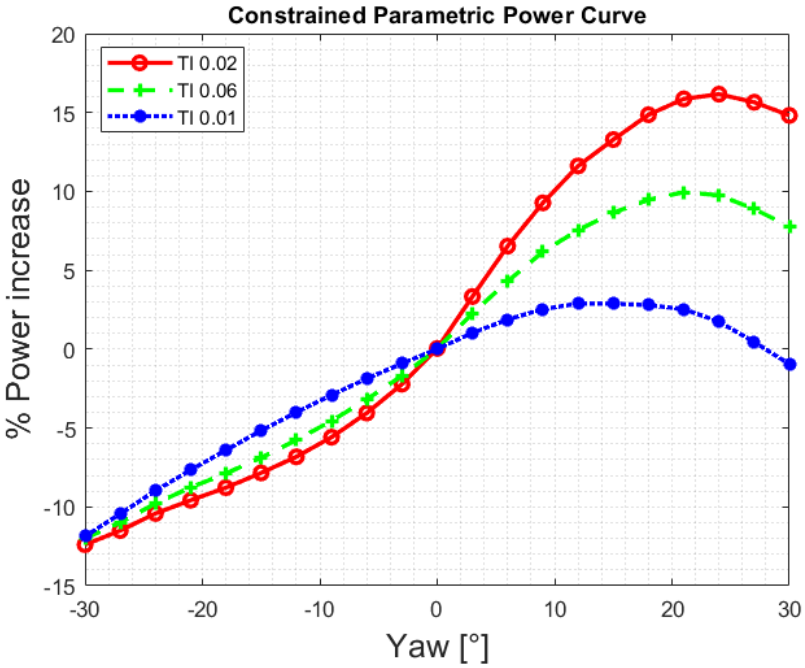

Figure A.4: Constrained parametric power curve example

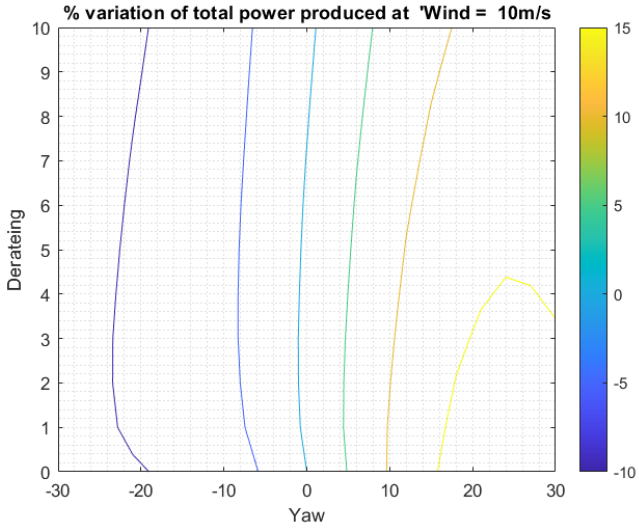

Figure A.5: Contour plot of the PPI surface expample

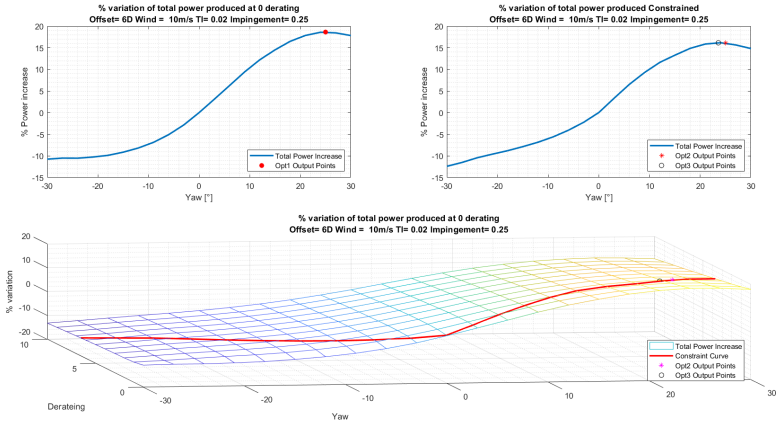

Figure A.6: Yaw only, constrained power curves and PPI surface example

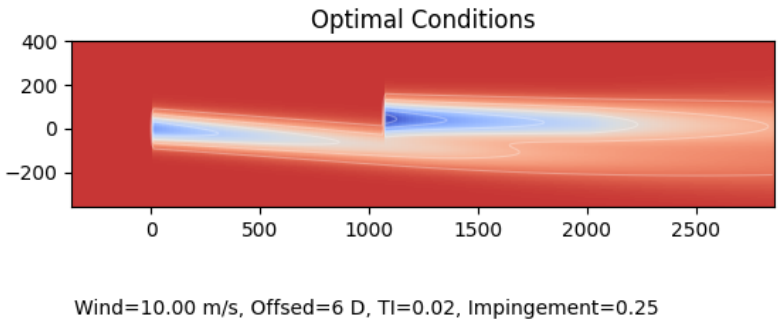

Figure A.7: FLORIS output example

The second window presents itself as shown in fig. A.8. This application allows the user to produce the optimal parametric trend curves. To do so, it is necessary to choose the baseline parameters from the dropdown menu. Once this is done, it is possible to choose the variable for the y-axis from the group inside the green box and the x-variable from the orange box. Hitting the run button will automatically generate all the parametric curves for each combination of selected variables. For example, selecting two x-variables and two y-variables will produce four output figures, four and four sixteen, and so on. Suppose one of the options in the blue box is selected. In that case, it is not necessary to select an x-variable as the histogram button produces all the histograms discussed in the thesis, and the available power plot is generated for all the parameters.

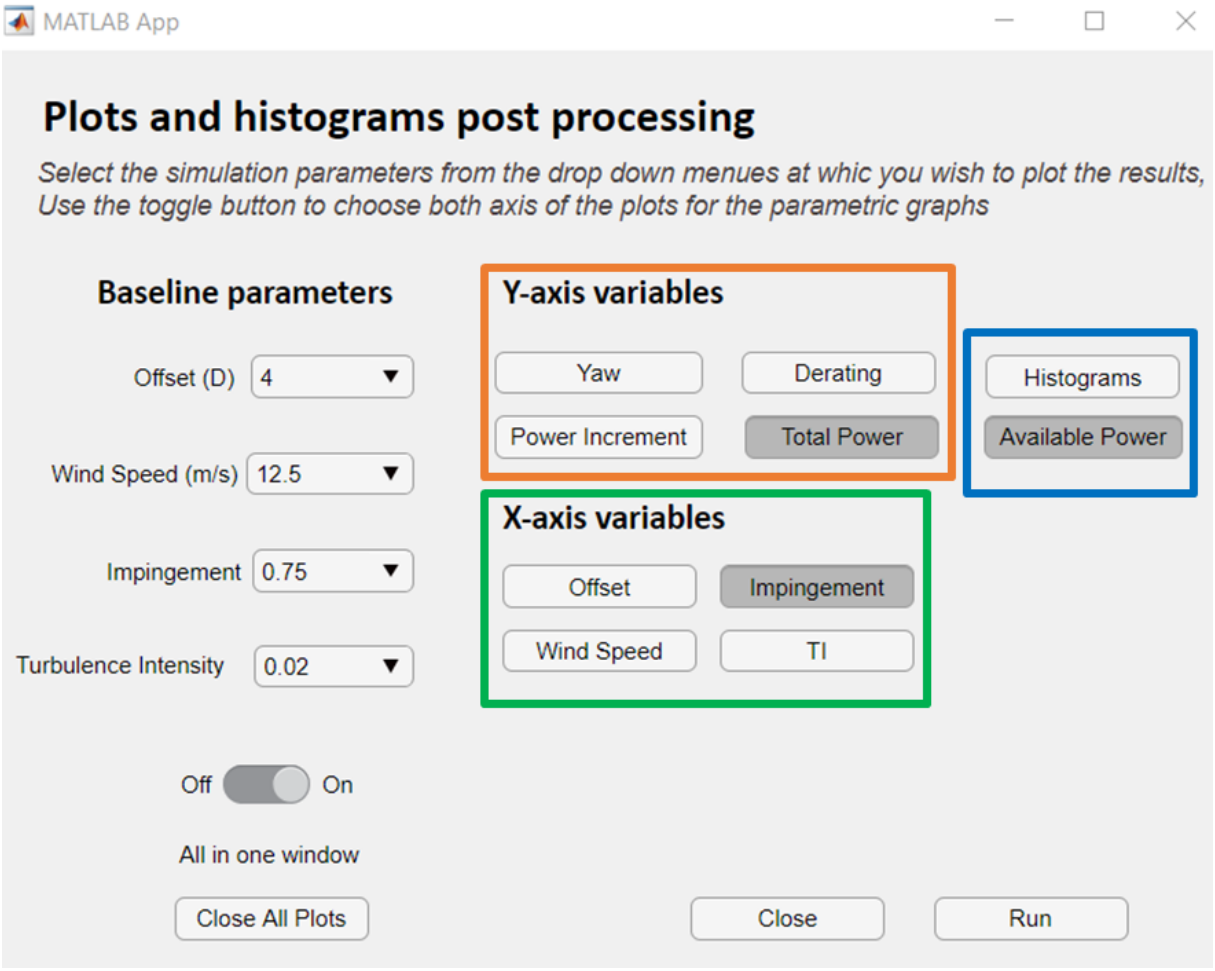

Figure A.8: Screenshot of the plot production app whit highlighted fields

Examples of these outputs have been shown throughout the thesis, but the following images show the product of hitting run in fig. A.8. The available power curve is in fig. A.9 while the parametric curve is in fig. A.10.

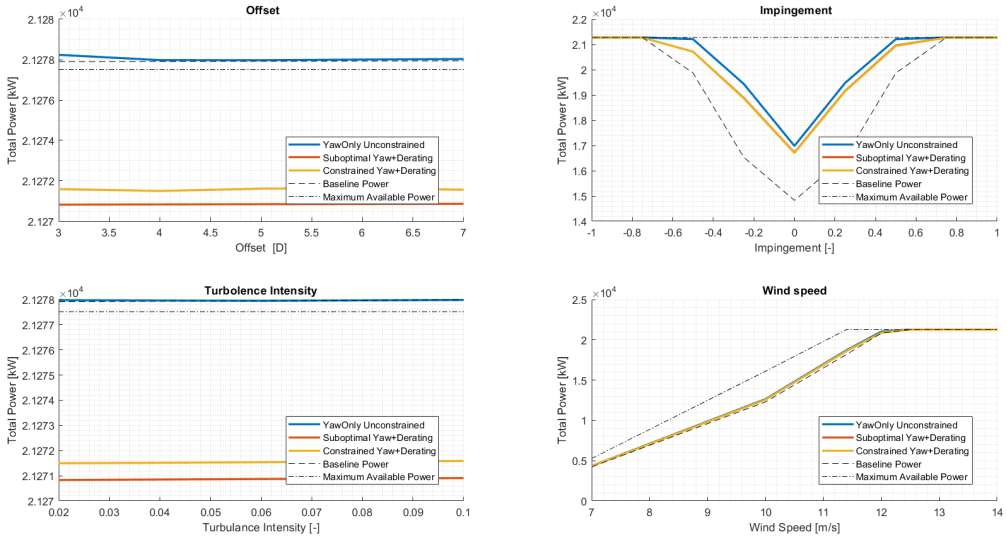

Figure A.9: Screenshot of the plot production app whit highlighted fields

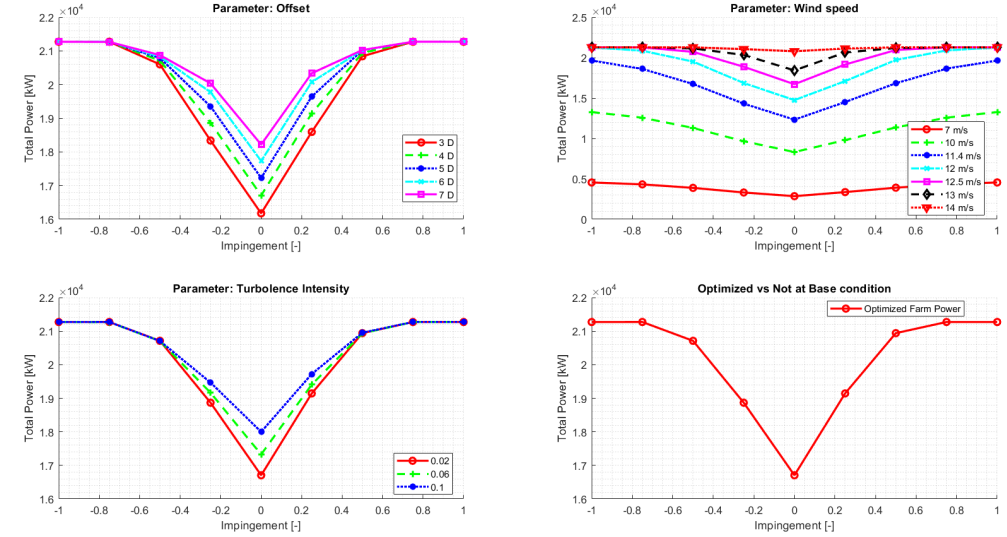

Figure A.10: Screenshot of the plot production app whit highlighted fields

List of Figures

1.1 *Fit for 55* info-graphic [6] detailing the goals for renewable energy in 2030 1
1.2 Lillground wind farm: variation in array efficiency with wind direction for wind speeds below rated. Credit to Dahlberg and Thor [11] 2

2.1 Demonstration of the yaw and tilt misalignment for wake steering. Credit to Gebraad et al. [12] 6
2.2 Summary of the results of the two-turbine simulation. Thanks to Fleming et al. [13] 7

3.1 Representation of the airfoils that constitute the DTU 10 MW turbine [14] 13
3.2 All the different wake modeling techniques implemented in FLORIS are applied to the same farm and their computational time [15] 14
3.3 Example of yaw-based steering strategy. Credit to Fleming et al. [17]. . . 16
3.4 Difference in reference values from the application of 15% derating. [1] . . 17
3.5 Block diagram representing the structure of the simulation script 18

4.1 DLCs simulated for the parametric analysis. Credits to Dadda G. [1] . . . 20
4.2 Derating needed to balance the effect of misalignment in function of the yaw angle.Blue line: maximum tip deflection. Red line: blade root combined ultimate load. [1] 20
4.3 The constraint curve computed based on data presented in [1] 21
4.4 Visualization of the geometric parameters of a wind farm at impingement 0.75 22
4.5 A representation of the global optimization domain, highlighting in orange the derating 0% that is the domain of the yaw-only sub-problem. 25
4.6 A typical power curve for derating 0% with the optimization results 25
4.7 Graphical representation of the construction of the solution of the suboptimal yaw+derating optimization problem starting from the solution of the yaw-only problem 27

4.8 The constraint curve is overlapped on the domain of the optimization problem revealing the feasible region; this is the domain of the constrained yaw+derating optimization problem 29

5.1 Contour plot of the PPI surface in Baseline conditions 33
5.2 3D surface graph of the PPI surface in Baseline conditions 33
5.3 0 Derating power curve in baseline conditions 34
5.4 Constrained power curve in baseline conditions 35
5.5 Parametric power curve over Impingement, Wind speed 11.4 m/s Offset 5 D TI 0.06 36
5.6 Constrained parametric power curve over Impingement, Wind speed 11.4 m/s Offset 5 D TI 0.06 37
5.7 Parametric power curve over Offset, Wind speed 11.4 m/s Impingement 0 D TI 0.06 38
5.8 Constrained parametric power curve over Offset, Wind speed 11.4 m/s Impingement 0 TI 0.06 39
5.9 Parametric power curve over Turbulence Intensity, Wind speed 11.4 m/s Impingement 0 Offset 5D 40
5.10 Constrained parametric power curve over Turbulence Intensity, Wind speed 11.4 m/s Impingement 0 Offset 5D 41
5.11 The power curve of a generic wind turbine. Credits A. Croce [18] 42
5.12 Parametric power curve over Wind Speed, TI 0.06 Impingement 0 Offset 5D 43
5.13 Constrained parametric power curve over Wind Speed, TI 0.06 Impingement 0 Offset 5D 44
5.14 3D surface graph of the PPI surface TI 0.06 Impingement 0 Offset 3D Wind 11.4 m/s 45
5.15 Contour plot of the PPI surface at TI 0.06 Impingement 0 Offset 3D Wind 11.4 m/s, with the constrained curve overlaid 46
5.16 Yaw-only power curve for Offset 5D, Wind speed 14 m/s, Impingement 0.25 and TI 0.06. 47
5.17 Constrained power curve for Offset 5D, Wind speed 14 m/s, Impingement 0.25 and TI 0.06. 48
5.18 Available power curve for Wind speed 11.4 m/s, Ti 0.06 and impingement 0 with offset as variable 50
5.19 Available power curve for Wind speed 11.4 m/s, Ti 0.06 and impingement 0 with offset as variable (zoomed). 50

5.20 Optimal yaw curve for Offset 5D, and TI 0.06 with wind speed as variable and impingement as a parameter. . . . 51
5.21 Optimal derating curve for Offset 5D, and TI 0.06 with wind speed as variable and impingement as a parameter. . . . 52
5.22 Total power curve for Wind speed 11.4 m/s, and TI 0.06 with Impingement as variable and offset as a parameter. . . . 53
5.23 Total power curve for Wind speed 11.4 m/s, and TI 0.06 with Impingement as variable and offset as a parameter (zoom). . . . 54
5.24 Total power curve for Wind speed 11.4 m/s, and impingement 1 with offset as variable and TI as a parameter. . . . 54
5.25 Representation of the flow field for impingement 1, offset 7D, wind speed 11.4 m/s and TI 0.02 . . . 55
5.26 Representation of the flow field for impingement 1, offset 7D, wind speed 11.4 m/s and TI 0.1 . . . 55
5.27 PPI curve for TI 0.06, and impingement 0 with wind speed as a variable and offset as a parameter. . . . 56
5.28 PPI curve for offset 5D, and impingement 0 with wind speed as a variable and TI as a parameter. . . . 57
5.29 Available power curve for TI 0.06, impingement 0, and offset 5D with wind speed as a variable. . . . 58
5.30 PPI curve for offset 5D, and TI 0.06 with wind speed as a variable and impingement as a parameter. . . . 58
5.31 PPI curve for offset 5D, and TI 0.06 with impingement as a variable and wind speed as a parameter. . . . 60
5.32 Histogram representation of the PPI of all three optimization strategies. . . 62
5.33 Histogram representation of the power difference between the unconstrained yaw-only strategy and the constrained yaw+derating . . . 63
5.34 Histogram representation of the power difference between the unconstrained yaw-only strategy and the suboptimal yaw+derating . . . 64
5.35 Histogram representation of the power difference between the constrained yaw+derating strategy and the suboptimal yaw+derating . . . 65
5.36 Histogram representation of yaw difference between the optimization strategies . . . 66

A.1 Complete overview of the optimization process . . . 74
A.2 Screenshot of the optimality verification app whit highlighted fields . . . 75
A.3 Yaw only parametric power curve example . . . 76

A.4 Constrained parametric power curve example 76
A.5 Contour plot of the PPI surface expample 77
A.6 Yaw only, constrained power curves and PPI surface example 77
A.7 FLORIS output example 77
A.8 Screenshot of the plot production app whit highlighted fields 78
A.9 Screenshot of the plot production app whit highlighted fields 79
A.10 Screenshot of the plot production app whit highlighted fields 79

List of Tables

2.1 List of the critical loads for a yawed turbine. Data credits to Dadda G. [1] 8
2.2 List of the critical loads for a derated turbine. Data credits to Dadda G. [1] 9

3.1 DTU 10 MW reference turbine main parameters. 12
3.2 List of airfoils on the DTU turbine. 12

List of Symbols

Variable	Description	SI unit
a	Axial induction factor	-
Π	Parameters Vector	[m/s, - , - , D, -]
J	Adimensional Power Function	-
P	Total Power	kW
$\bar{P}$	Baseline Power	kW
$\widehat{\Phi}$	Adimensional Yaw angle	-
Φ	Yaw Angle	$^\circ$
F	Yaw adimensionalization factor	$^\circ$
ξ	Derating	-
PPI	Percentage Power Increase	%
ρ	Air density	kg/m^3
A	Rotor surface	m^2
C_p	Power Coefficient	-
C_t	Thrust Coefficient	-
V	Wind Speed	m/s
λ	Tip speed ratio	-
$\lambda*$	Optimal tip speed ratio	-